



# 1 Aqueous SOA formation from the photo-oxidation of vanillin: Direct 2 photosensitized reactions and nitrate-mediated reactions

3 Brix Raphael Go<sup>1</sup>, Yan Lyu<sup>1</sup>, Yan Ji<sup>1</sup>, Dan Dan Huang<sup>2</sup>, Xue Li<sup>3</sup>, Theodora Nah<sup>1</sup>, Chun Ho  
4 Lam<sup>1</sup>, and Chak K. Chan<sup>1\*</sup>

5 <sup>1</sup>School of Energy and Environment, City University of Hong Kong, Hong Kong, China

6 <sup>2</sup>Shanghai Academy of Environmental Sciences, Shanghai 200233, China

7 <sup>3</sup>Institute of Mass Spectrometry and Atmospheric Environment, Jinan University No. 601 Huangpu Avenue West,  
8 Guangzhou 510632, China

9

10 *Correspondence to:* Chak K. Chan (Chak.K.Chan@cityu.edu.hk)

11 **Abstract.** Vanillin (VL), a phenolic aromatic carbonyl abundant in biomass burning emissions, forms triplet excited states  
12 (<sup>3</sup>VL\*) under simulated sunlight leading to aqueous secondary organic aerosol (aqSOA) formation. This direct  
13 photosensitized oxidation of VL was compared with nitrate-mediated VL photo-oxidation under atmospherically relevant  
14 cloud and fog conditions, through examining the VL decay kinetics, product compositions, and light absorbance changes.  
15 The majority of the most abundant products from both VL photo-oxidation pathways were potential Brown carbon (BrC)  
16 chromophores. In addition, both pathways generated oligomers, functionalized monomers, and oxygenated ring-opening  
17 products, but nitrate promoted functionalization and nitration, which can be ascribed to its photolysis products (<sup>•</sup>OH, <sup>•</sup>NO<sub>2</sub>,  
18 and N(III), NO<sub>2</sub><sup>-</sup> or HONO). Moreover, a potential imidazole derivative observed from nitrate-mediated VL photo-oxidation  
19 suggested that ammonium may be involved in the reactions. The effects of secondary oxidants from <sup>3</sup>VL\*, pH, the presence  
20 of volatile organic compounds (VOCs) and inorganic anions, and reactants concentration and molar ratios on VL photo-  
21 oxidation were also explored. Our findings show that the secondary oxidants (<sup>1</sup>O<sub>2</sub>, O<sub>2</sub><sup>-</sup>/<sup>•</sup>HO<sub>2</sub>, <sup>•</sup>OH) from the reactions of  
22 <sup>3</sup>VL\* and O<sub>2</sub> play an essential role in VL photo-oxidation. Enhanced oligomer formation was noted at pH <4 and in the  
23 presence of VOCs and inorganic anions, probably due to additional generation of radicals (<sup>•</sup>HO<sub>2</sub> and CO<sub>3</sub><sup>-</sup>). Also,  
24 functionalization was dominant at low VL concentration, whereas oligomerization was favored at high VL concentration.  
25 Furthermore, guaiacol oxidation by photosensitized reactions of VL was observed to be more efficient relative to nitrate-  
26 mediated photo-oxidation. Lastly, potential VL photo-oxidation pathways under different reaction conditions were proposed.  
27 This study indicates that the direct photosensitized oxidation of VL, which nitrate photolysis products can further enhance,  
28 may be an important aqSOA source in areas influenced by biomass burning emissions.



## 29 1 Introduction

30 Aqueous reactions can be an important source of secondary organic aerosols (SOA) (Blando and Turpin, 2000; Volkamer et  
31 al., 2009; Lim et al., 2010; Ervens et al., 2011; Huang et al., 2011; Lee et al., 2011; Smith et al., 2014) such as highly-  
32 oxygenated and low-volatility organics (Hoffmann et al., 2018; Liu et al., 2019) which may affect aerosol optical properties  
33 due to contributions to Brown Carbon (BrC) (Gilardoni et al., 2016). BrC refers to organic aerosols that absorb radiation  
34 efficiently in the near-ultraviolet (UV) and visible regions (Laskin et al., 2015). The formation of aqueous SOA (aqSOA) via  
35 photochemical reactions involves oxidation, with hydroxyl radical ( $\cdot\text{OH}$ ) usually considered as the primary oxidant  
36 (Herrmann et al., 2010; Smith et al., 2014). The significance of photosensitized chemistry in atmospheric aerosols has  
37 recently been reviewed (George et al., 2015). For instance, triplet excited states of organic compounds ( $^3\text{C}^*$ ) from the  
38 irradiation of light-absorbing organics such as non-phenolic aromatic carbonyls (Canonica et al., 1995; Anastasio et al.,  
39 1996; Vione et al., 2006; Smith et al., 2014) have been reported to oxidize phenols at faster rates and with higher aqSOA  
40 yields compared to  $\cdot\text{OH}$  (Sun et al., 2010; Smith et al., 2014; Yu et al., 2014; Smith et al., 2016). Aside from being an  
41 oxidant,  $^3\text{C}^*$  can also be a precursor of singlet oxygen ( $^1\text{O}_2$ ), superoxide ( $\text{O}_2^{\cdot-}$ ) or hydroperoxyl ( $\cdot\text{HO}_2$ ) radical, and  $\cdot\text{OH}$  (via  
42  $\text{HO}_2^{\cdot}/\text{O}_2^{\cdot-}$  formation) upon reactions with  $\text{O}_2$  and substrates (e.g., phenols), respectively (Tinel et al., 2018). The  $^3\text{C}^*$   
43 concentration in typical fog water has been estimated to be >25 times than that of  $\cdot\text{OH}$ , making  $^3\text{C}^*$  the primary photo-  
44 oxidant for biomass burning phenolic compounds (Kaur and Anastasio, 2018; Kaur et al., 2019). Recent works on triplet-  
45 driven oxidation of phenols have mainly focused on changes of physicochemical properties (e.g., light absorption) and  
46 aqSOA yield (e.g., Smith et al., 2014, 2015, 2016), with few reports on reaction mechanisms and characterization of reaction  
47 products (e.g., Yu et al., 2014; Chen et al., 2020; Jiang et al., 2021).

48 Inorganic nitrate is a major component of aerosols and cloud/fog water. In cloud and fog water, the concentrations  
49 of inorganic nitrate can vary from 50  $\mu\text{M}$  to >1000  $\mu\text{M}$ , with higher levels typically noted under polluted conditions (Munger  
50 et al., 1983; Collett et al., 1998; Zhang and Anastasio, 2003; Li et al., 2011; Giulianelli et al., 2014; Bianco et al., 2020).  
51 Upon photolysis (Vione et al., 2006; Herrmann, 2007; Scharko et al., 2014), inorganic nitrate in cloud and fog water can  
52 contribute to BrC (Minero et al., 2007) and aqSOA formation (Huang et al., 2018; Klodt et al., 2019; Zhang et al., 2021) by  
53 generating  $\cdot\text{OH}$  and nitrating agents (e.g.,  $\cdot\text{NO}_2$ ). For example, the aqSOA yields from the photo-oxidation of phenolic  
54 carbonyls in nitrate are twice as high as that in sulfate solution (Huang et al., 2018). Nitration is a significant process in the  
55 formation of light-absorbing organics or BrC in the atmosphere (Jacobson, 1999; Kahnt et al., 2013; Mohr et al., 2013;  
56 Laskin et al., 2015; Teich et al., 2017; Li et al., 2020). Furthermore, nitrate photolysis has been proposed to be a potentially  
57 important process for  $\text{SO}_2$  oxidation via the generation of  $\cdot\text{OH}$ ,  $\cdot\text{NO}_2$ , and N(III) within particles (Gen et al., 2019a, 2019b),  
58 and it can also potentially change the morphology of atmospheric viscous particles (Liang et al., 2021). Accordingly, both  
59  $^3\text{C}^*$  and inorganic nitrate can contribute to aqSOA and BrC formation.

60 Biomass burning (BB) is a significant atmospheric source of both phenolic and non-phenolic aromatic carbonyls  
61 (Rogge et al., 1998; Nolte et al., 2001; Schauer et al., 2001; Bond et al., 2004). An example is vanillin (VL) (Henry's law



62 constant of  $4.56 \times 10^5 \text{ M atm}^{-1}$ ; Yaws, 1994), a model compound for methoxyphenols which are abundant in BB emissions  
63 (Pang et al., 2019a), which has been shown to yield low-volatility products (Li et al., 2014) via aqueous  $\cdot\text{OH}$  oxidation and  
64 direct photodegradation. Photodegradation kinetics and aqSOA yields have been reported for direct VL photodegradation  
65 (Smith et al., 2016), with oxygenated aliphatic-like compounds (high H:C,  $\geq 1.5$  and low O:C,  $\leq 0.5$  ratios) reported as the  
66 most likely products (Loisel et al., 2021). Additionally, aqueous-phase reactions of phenols with reactive nitrogen species  
67 have been proposed to be a significant source of nitrophenols and SOA (Grosjean, 1985; Kitanovski et al., 2014; Kroflić et  
68 al., 2015; Pang et al., 2019a; Kroflić et al., 2021; Yang et al., 2021). For instance, nitrite-mediated VL photo-oxidation can  
69 generate nitrophenols, and the reactions are influenced by nitrite/VL molar ratios, pH, and the presence of  $\cdot\text{OH}$  scavengers  
70 (Pang et al., 2019a).

71 As BB aerosols are typically internally mixed with other aerosol components (Zielinski et al., 2020), VL may  
72 coexist with nitrate in BB aerosols. The aqueous-phase photo-oxidation of VL and nitrate may then reveal insights into the  
73 atmospheric processing of BB aerosols. In addition, pollution from large BB events in central Amazonia has been reported to  
74 interact with volatile organic compounds (VOCs) and soil dust (Rizzo et al., 2010). Moreover, the production, growth, and  
75 chemical complexity of SOA can be influenced by the uptake and aerosol-phase reactions of VOCs (Pöschl, 2005; De Gouw  
76 and Jimenez, 2009; Ziemann and Atkinson, 2012). Accordingly, studies incorporating other atmospherically relevant species  
77 (e.g., VOCs and inorganic anions) in photo-oxidation experiments are warranted.

78 To evaluate the potential significance of VL and its reactions with nitrate in aqSOA formation in cloud/fog water,  
79 we studied the direct photosensitized oxidation of VL and nitrate-mediated VL photo-oxidation under atmospherically  
80 relevant conditions. In this work, reactions were characterized based on VL decay kinetics, light absorbance changes, and  
81 products. The influences of secondary oxidants from VL triplets, solution pH, the presence of VOCs and inorganic anions,  
82 and reactants concentration and molar ratios on these two photo-oxidation pathways were also assessed. The  $^3\text{C}^*$  of non-  
83 phenolic aromatic carbonyls (e.g., 3-4-dimethoxybenzaldehyde, DMB; a non-phenolic aromatic carbonyl) (Smith et al.,  
84 2014; Yu et al., 2014; Jiang et al., 2021) and phenolic aromatic carbonyls (e.g., acetosyringone, vanillin) (Smith et al., 2016)  
85 have been shown to oxidize phenols, but the reaction products from the latter are unknown. We then examined the photo-  
86 oxidation of guaiacol, another non-carbonyl phenol, in the presence of VL and compared it with nitrate-mediated photo-  
87 oxidation. Finally, we proposed photo-oxidation pathways of VL under different reaction conditions. This work presents a  
88 comprehensive comparison of VL photo-oxidation by VL photosensitization and in the presence of inorganic nitrate.

89

## 90 **2 Methods**

### 91 **2.1 Aqueous phase photo-oxidation experiments**

92 Photo-oxidation experiments were performed in a 500-mL custom-built quartz photoreactor equipped with a magnetic  
93 stirrer. The solutions were bubbled with synthetic air or nitrogen ( $\text{N}_2$ ) (>99.995%) for 30 min before irradiation to achieve



94 air- and N<sub>2</sub>-saturated conditions, respectively, and the bubbling was continued throughout the reactions (Du et al., 2011;  
95 Chen et al., 2020). The aim of the air-saturated experiments was to enable the generation of secondary oxidants (<sup>1</sup>O<sub>2</sub>, O<sub>2</sub><sup>•</sup>  
96 /HO<sub>2</sub>, <sup>•</sup>OH) from <sup>3</sup>VL\* as O<sub>2</sub> is present. Conversely, the N<sub>2</sub>-saturated experiments would inhibit the formation of these  
97 secondary oxidants, leading to <sup>3</sup>VL\*-driven reactions. Solutions were irradiated through the quartz window of the reactor  
98 using a xenon lamp (model 6258, Ozone free xenon lamp, 300 W, Newport) equipped with a longpass filter (20CGA-305 nm  
99 cut-on filter, Newport) to eliminate light below 300 nm. Cooling fans positioned around the photoreactor and lamp housing  
100 maintained reaction temperatures at 27±2 °C. The averaged initial photon flux in the reactor from 300 to 380 nm measured  
101 using a chemical actinometer (2-nitrobenzaldehyde) was 2.6×10<sup>15</sup> photons cm<sup>-2</sup> s<sup>-1</sup> nm<sup>-1</sup> (Fig. S1). Although the  
102 concentration of VL in cloud/fog water has been estimated to be <0.01 mM (Anastasio et al., 1996), a higher VL  
103 concentration (0.1 mM) was used in this study to guarantee sufficient signals for product identification (Vione et al., 2019).  
104 The chosen ammonium nitrate (AN) concentration (1 mM) was based on values observed in cloud and fog water (Munger et  
105 al., 1983; Collett et al., 1998; Zhang and Anastasio, 2003; Li et al., 2011; Giulianelli et al., 2014; Bianco et al., 2020). We  
106 also examined the role of VOCs (2-propanol, IPA) (1 mM) and inorganic anions (sodium bicarbonate, NaBC) (1 mM) in  
107 these reactions. IPA can be classified as both a biogenic (from grass, Olofsson et al., 2003) and anthropogenic VOC (e.g.,  
108 from solvents and industrial processes, Hippelein, 2004; Lewis et al., 2020), while bicarbonate is an inorganic anion  
109 observed in fog water from both urban and rural locations (Collett et al., 1999; Straub et al., 2012; Straub, 2017). IPA and  
110 NaBC are particularly interesting also because they can produce other radicals (e.g., <sup>•</sup>HO<sub>2</sub> and carbonate radical, CO<sub>3</sub><sup>•</sup>) that  
111 may react with nitrate photolysis products (Vione et al., 2009; Wang et al., 2021) and they can act as <sup>•</sup>OH scavengers  
112 (Warneck and Wurzinger, 1988; Vione et al., 2009; Gen et al., 2019b; Pang et al., 2019a), although it must be noted that  
113 these compounds were not added in excess for our experiments. Moreover, comparisons were made between the photo-  
114 oxidation of guaiacol (0.1 mM), a non-carbonyl phenol, in the presence of VL (0.1 mM) or AN (1 mM). Samples (10 mL)  
115 were collected hourly for a total of 6 h for offline optical and chemical analyses. Absorbance measurements, VL (and GUA)  
116 decay kinetics (calibration curves for VL and GUA standard solutions; Fig. S2), small organic acids measurements, and  
117 product characterization were conducted using UV-Vis spectrophotometry, ultra-high-performance liquid chromatography  
118 with photodiode array detector (UHPLC-PDA), ion chromatography (IC), and UHPLC coupled with quadrupole time-of-  
119 flight mass spectrometry (UHPLC-qToF-MS) equipped with an electrospray ionization (ESI) source and operated in the  
120 positive ion mode (the negative ion mode signals were too low for our analyses), respectively. Each experiment was repeated  
121 independently at least three times and measurements were done in triplicate. Details on the materials and analytical  
122 procedures are provided in the Supporting Information (Text S1 to S6). The pseudo-first-order rate constant (*k'*) for VL  
123 decay was determined using the following equation (Huang et al., 2018):

$$\ln ([\text{VL}]_t / [\text{VL}]_0) = -k't \quad (\text{Eq. 1})$$

124  
125  
126



127 where  $[VL]_t$  and  $[VL]_0$  are the concentrations of VL at time  $t$  and 0, respectively. Replacing VL with GUA in Eq. 1 enabled  
128 the calculation of GUA decay.

## 129 2.2 Calculation of normalized abundance of products

130 The normalized abundance of a product, [P] (unitless), was calculated as follows:

$$131 \quad [P] = \frac{A_{P,t}}{A_{VL,t}} \cdot \frac{[VL]_t}{[VL]_0} \quad (\text{Eq. 2})$$

132 where  $A_{P,t}$  and  $A_{VL,t}$  are the extracted ion chromatogram (EIC) signal peak areas of the product P and VL from UHPLC-  
133 qToF-MS analyses at time  $t$ , respectively;  $[VL]_t$  and  $[VL]_0$  are the VL concentrations ( $\mu\text{M}$ ) determined using UHPLC at time  
134  $t$  and 0, respectively. Here, we relied on the more accurate measurements of [VL] using UHPLC for semi-quantification. It  
135 should be noted that the ionization efficiency may greatly vary for different classes of compounds (Kearle, 2000). Hence,  
136 we assumed equal ionization efficiency of different compounds to calculate their normalized abundance, which is commonly  
137 used to estimate O:C ratios of SOA (Bateman et al., 2012; Lin et al., 2012; De Haan et al., 2019). Typical fragmentation  
138 behavior observed in MS/MS spectra for individual functional groups from Holčápek et al. (2010) are outlined in Table S1.  
139

## 140 3 Results and Discussion

### 141 3.1 Kinetics, mass spectrometric, and absorbance changes analyses during aqueous phase photo-oxidation of vanillin

142 Table S2 summarizes the reaction conditions, initial VL (and GUA) decay rates, normalized abundance of products, and  
143 average carbon oxidation state ( $\langle\text{OS}_c\rangle$ ) (of the 50 most abundant products). In general, the 50 most abundant products  
144 contributed more than half of the total normalized abundance of products. For clarity purposes, the reactions involving  
145 reactive species referred to in the following discussions are provided in Table 1.

146 As shown in Figure S3, VL underwent oxidation both directly and in the presence of nitrate upon simulated sunlight  
147 illumination. VL absorbs light and is promoted to its excited singlet state ( $^1\text{VL}^*$ ), then undergoes intersystem crossing (ISC)  
148 to the excited triplet state,  $^3\text{VL}^*$ . In principle,  $^3\text{VL}^*$  can oxidize ground-state VL (Type I photosensitized reactions) via H-  
149 atom abstraction/electron transfer and form  $\text{O}_2^{\cdot-}$  or  $\text{HO}_2^{\cdot}$  in the presence of  $\text{O}_2$  (Tinel et al., 2018), or react with  $\text{O}_2$  (Type II  
150 photosensitized reactions) to yield  $^1\text{O}_2$  via energy transfer or  $\text{O}_2^{\cdot-}$  via electron transfer (Lee et al., 1987; Foote et al., 1991).  
151 The disproportionation of  $\text{HO}_2^{\cdot}/\text{O}_2^{\cdot-}$  (Anastasio et al., 1996) and reaction of  $\text{HO}_2^{\cdot}$  with  $\text{O}_2^{\cdot-}$  (Du et al., 2011) form hydrogen  
152 peroxide ( $\text{H}_2\text{O}_2$ ), which is a photolytic source of  $^{\cdot}\text{OH}$ . Overall, air-saturated conditions, in which  $\text{O}_2$  is present, enable the  
153 generation of secondary oxidants from  $^3\text{VL}^*$  ( $^1\text{O}_2$ ,  $\text{O}_2^{\cdot-}/\text{HO}_2^{\cdot}$ ,  $^{\cdot}\text{OH}$ ). Moreover,  $^{\cdot}\text{OH}$ ,  $^{\cdot}\text{NO}_2$ , and  $\text{NO}_2/\text{HNO}_2$ , i.e., N(III),  
154 generated via nitrate photolysis (Reactions 1-3; Table 1) can also oxidize or nitrate VL. In this work, the direct  
155 photosensitized oxidation of VL (by  $^3\text{VL}^*$  or secondary oxidants from  $^3\text{VL}^*$  and  $\text{O}_2$ ) and nitrate-mediated VL photo-  
156 oxidation are referred to as VL\* and VL+AN, respectively.



### 157 3.1.1 Effect of secondary oxidants from VL triplets

158 As mentioned earlier, secondary oxidants ( $^1\text{O}_2$ ,  $\text{O}_2^{\cdot-}/\text{HO}_2$ ,  $\cdot\text{OH}$ ) can be generated from  $^3\text{VL}^*$  when  $\text{O}_2$  is present (e.g., under  
159 air-saturated conditions), while  $^3\text{VL}^*$  is the only oxidant expected under  $\text{N}_2$ -saturated conditions. To examine the  
160 contributions of  $^3\text{VL}^*$ -derived secondary oxidants and  $^3\text{VL}^*$  only on VL photo-oxidation, experiments under both air- and  
161  $\text{N}_2$ -saturated conditions (Fig. S3a) were carried out at pH 4, which is representative of moderately acidic aerosol and cloud  
162 pH values (Pye et al., 2020). No significant VL loss was observed for dark experiments. The low decay rate for  $\text{VL}^*$  under  
163  $\text{N}_2$ -saturated conditions suggests a minimal role for  $^3\text{VL}^*$  in VL photo-oxidation. Contrastingly, the  $\text{VL}^*$  decay rate under  
164 air-saturated conditions was 4 times higher, revealing the importance of  $^3\text{VL}^*$ -derived secondary oxidants for  
165 photosensitized oxidation of VL. Aside from  $\cdot\text{OH}$ ,  $\text{O}_2^{\cdot-}/\text{HO}_2$  and  $^1\text{O}_2$  can also promote VL photo-oxidation (Kaur and  
166 Anastasio, 2018; Chen et al., 2020).  $^1\text{O}_2$  is also an efficient oxidant for unsaturated organic compounds and has a lifetime that  
167 is much longer than  $^3\text{C}^*$  (Chen et al., 2020). Similar to  $\text{VL}^*$ , the decay rate for  $\text{VL}+\text{AN}$  under air-saturated conditions was  
168 faster (6.6 times) than  $\text{N}_2$ -saturated conditions, which can be due to several reactions facilitated by nitrate photolysis  
169 products and the enhancement of N(III)-mediated photo-oxidation in the presence of  $\text{O}_2$  as reported in early works (Vione et  
170 al., 2005; Kim et al., 2014; Pang et al., 2019a). An example is enhanced VL nitration likely from increased  $\cdot\text{NO}_2$  formation  
171 such as from the reaction of  $\cdot\text{OH}$  and  $\text{O}_2^{\cdot-}$  with  $\text{NO}_2^-$  (Reactions 4 and 5, respectively; Table 1) or the autoxidation of  $\cdot\text{NO}$   
172 from  $\text{NO}_2^-$  photolysis (Reactions 6-9; Table 1) in aqueous solutions (Pang et al., 2019a). Reactions involving  $\cdot\text{HO}_2/\text{O}_2^{\cdot-}$  which  
173 may originate from the photolysis of nitrate alone, likely from the production and subsequent photolysis of peroxyxynitrous  
174 acid ( $\text{HOONO}$ ) (Reaction 10; Table 1) (Jung et al., 2017; Wang et al., 2021), or the reactions of  $^3\text{VL}^*$  in the presence of  $\text{O}_2$ ,  
175 may have contributed as well. For instance, Wang et al. (2021) recently demonstrated that nitrate photolysis generates  
176  $\cdot\text{HO}_2/\text{O}_2^{\cdot-}(\text{aq})$  and  $\text{HONO}(\text{g})$  in the presence of dissolved aliphatic organic matter (e.g., nonanoic acid, ethanol), with the  
177 enhanced  $\text{HONO}(\text{g})$  production caused by secondary photochemistry between  $\cdot\text{HO}_2/\text{O}_2^{\cdot-}(\text{aq})$  and photoproducted  $\text{NO}_{x(\text{aq})}$   
178 (Reactions 11 and 12; Table 1), in agreement with Scharko et al. (2014). The significance of this increased HONO  
179 production is enhanced  $\cdot\text{OH}$  formation (Reaction 13; Table 1). In addition,  $\cdot\text{HO}_2$  can react with  $\cdot\text{NO}$  (Reaction 10; Table 1)  
180 from  $\text{NO}_2^-$  photolysis (Reaction 6; Table 1) to form  $\text{HOONO}$ , and eventually  $\cdot\text{NO}_2$  and  $\cdot\text{OH}$  (Reaction 14; Table 1) (Pang et  
181 al., 2019a). Nevertheless, the comparable decay rates for  $\text{VL}^*$  and  $\text{VL}+\text{AN}$  imply that  $\text{VL}^*$  chemistry still dominates even at  
182 1:10 molar ratio of VL/nitrate, probably due to the much higher molar absorptivity of VL compared to that of nitrate (Fig.  
183 S1) and the high VL concentration (0.1 mM) used in this study. Although we have no quantification of the oxidants in our  
184 reaction systems as it is outside the scope of this study, these observations clearly substantiate that secondary oxidants from  
185  $^3\text{VL}^*$ , which are formed when  $\text{O}_2$  is present, are required for efficient photosensitized oxidation of VL and nitrate-mediated  
186 VL photo-oxidation.

187 The products from  $\text{VL}^*$  under  $\text{N}_2$ -saturated conditions were mainly oligomers (e.g.,  $\text{C}_{16}\text{H}_{14}\text{O}_4$ ) (Fig. 1a), consistent  
188 with triplet-mediated oxidation forming higher molecular weight products, probably with less fragmentation relative to  
189 oxidation by  $\cdot\text{OH}$  (Chen et al., 2020). A threefold increase in the normalized abundance of products was noted upon addition





190 of nitrate (VL+AN under N<sub>2</sub>-saturated conditions; Fig. 1b), and in addition to oligomers, functionalized monomers (e.g.,  
191 C<sub>8</sub>H<sub>6</sub>O<sub>5</sub>) and nitrogen-containing compounds (e.g., C<sub>8</sub>H<sub>9</sub>NO<sub>3</sub>; No. 2, Table S3) were also observed, in agreement with <sup>•</sup>OH-  
192 initiated oxidation yielding more functionalized/oxygenated products compared to triplet-mediated oxidation (Chen et al.,  
193 2020). Compared to N<sub>2</sub>-saturated conditions, the normalized abundance of products such as oligomers and functionalized  
194 monomers (e.g., demethylated VL; Fig. S4) were significantly higher under air-saturated conditions (Figs. 1c-d), likely due  
195 to the secondary oxidants from <sup>3</sup>VL\* and O<sub>2</sub> and their interactions with nitrate photolysis products. The nitrogen-containing  
196 compounds (e.g., C<sub>16</sub>H<sub>10</sub>N<sub>2</sub>O<sub>9</sub>; No. 3, Table S3) were also more relatively abundant under air-saturated conditions. For both  
197 VL\* and VL+AN under air-saturated conditions, the most abundant product was C<sub>10</sub>H<sub>10</sub>O<sub>5</sub> (No. 4, Table S3), a substituted  
198 VL. Irradiation of VL by 254-nm has also been reported to lead to VL dimerization and functionalization via ring-retaining  
199 pathways, as well as small oxygenates but only when <sup>•</sup>OH from H<sub>2</sub>O<sub>2</sub> were involved (Li et al., 2014). In this work, small  
200 organic acids were observed from both VL\* and VL+AN under air-saturated conditions (Fig. S5) due to simulated sunlight  
201 that could access the 308-nm VL band (Smith et al., 2016). Interestingly, we observed a potential imidazole derivative  
202 (C<sub>5</sub>H<sub>5</sub>N<sub>3</sub>O<sub>2</sub>; Fig. 1d) from VL+AN under air-saturated conditions, which may have formed from reactions induced by  
203 ammonium. This compound was not observed in a parallel experiment in which AN was replaced with sodium nitrate (SN)  
204 (Fig. S6a; see Sect. 3.3 for discussion). The molecular transformation of VL upon photo-oxidation was examined using the  
205 van Krevelen diagrams (Fig. S7). For all experiments (A1-19; Table S2) in this study, the O:C and H:C ratios of the products  
206 were mainly similar to those observed from the aging of other phenolics (Yu et al., 2014) and BB aerosols (Qi et al., 2019).  
207 Oligomers with O:C ratios ≤0.6 were dominant in VL\* under N<sub>2</sub>-saturated conditions. For VL+AN under N<sub>2</sub>-saturated  
208 conditions, smaller molecules (n<sub>c</sub> ≤8) with higher O:C ratios (up to 0.8) were also observed. More products with higher O:C  
209 ratios (≥0.6) were noted under air-saturated conditions for both VL\* and VL+AN. The H:C ratios were mostly around 1.0,  
210 indicating that the products for experiments A5 to A8 (Table S2) were mainly aromatic species. Compounds with H:C ≤1.0  
211 and O:C ≤0.5 are common for aromatic species, while compounds with H:C ≥1.5 and O:C ≤0.5 are typical for more aliphatic  
212 species (Mazzoleni et al., 2012; Kourtchev et al., 2014; Jiang et al., 2021). Moreover, majority of the products for  
213 experiments A5 to A8 have double bond equivalent (DBE) values >7, which corresponds to oxidized aromatic compounds  
214 (Xie et al., 2020). In contrast, Loisel et al. (2021) reported mainly oxygenated aliphatic-like compounds (H:C, ≥1.5 and O:C,  
215 ≤0.5 ratios) from the direct irradiation of VL (0.1 mM), which may be due to their use of ESI in the negative ion mode,  
216 which has higher sensitivity for detecting compounds such as carboxylic acids (Holčapek et al., 2010; Lüigand et al., 2017)  
217 and solid-phase extraction (SPE) procedure causing the loss of some oligomers (LeClair et al., 2012; Zhao et al., 2013;  
218 Bianco et al., 2018). Among experiments A5 to A8 (Table S2), VL+AN under air-saturated conditions (A7) had the highest  
219 normalized abundance of products and <OS<sub>c</sub>>, most probably due to the combined influence of the secondary oxidants from  
220 <sup>3</sup>VL\* and O<sub>2</sub>, and nitrate photolysis products. In our calculations, the increase in <OS<sub>c</sub>> (except for VOCs and inorganic  
221 anions experiments; A9 to A12; Table S2) was lower than those in <sup>•</sup>OH- or triplet-mediated oxidation of phenolics (e.g.,  
222 phenol, guaiacol) measured using an aerosol mass spectrometer (Sun et al., 2010; Yu et al., 2014), likely because we  
223 excluded contributions from ring-opening products which may have higher OS<sub>c</sub> values as these products are not detectable in



224 the positive ion mode. Thus, the  $\langle \text{OS}_c \rangle$  in this study likely were lower estimates. In brief, the secondary oxidants from  $^3\text{VL}^*$   
225 and  $\text{O}_2$  increased the abundance of products and promoted the formation of more oxidized aqSOA. These trends were  
226 reinforced in the presence of nitrate, indicating synergistic effects between secondary oxidants from VL triplets and nitrate  
227 photolysis products.

228 Illumination of phenolic aromatic carbonyls with high molar absorptivities ( $\epsilon_{\lambda, \text{max}}$ ) ( $\sim 8$  to  $22 \times 10^3 \text{ M}^{-1} \text{ cm}^{-1}$ ) leads to  
229 an overall loss of light absorption but increased absorbance at longer wavelengths ( $>350 \text{ nm}$ ), where the carbonyls did not  
230 initially absorb light (Smith et al., 2016). Fig. 2a illustrates the changes in total absorbance from 350 to 550 nm of  $\text{VL}^*$  and  
231  $\text{VL}+\text{AN}$  under air- and  $\text{N}_2$ -saturated conditions. The absorption spectra of  $\text{VL}^*$  under air- and  $\text{N}_2$ -saturated conditions (pH  
232 4) at different time intervals are shown in Fig. S8. For both  $\text{VL}^*$  and  $\text{VL}+\text{AN}$ , evident absorbance enhancement was  
233 observed under air-saturated conditions, while the absorbance changes under  $\text{N}_2$ -saturated conditions were minimal,  
234 consistent with the VL decay trends. This absorbance enhancement can be explained by the formation of oligomers with  
235 large, conjugated  $\pi$ -electron systems (Chang and Thompson, 2010) and hydroxylated products (Li et al., 2014; Zhao et al.,  
236 2015), in agreement with the observed reaction products. In this work, phenoxy radicals can be generated from several  
237 processes such as the oxidation (Vione et al., 2019) of ground-state VL by  $^3\text{VL}^*$  via H-atom abstraction (Huang et al., 2018)  
238 and photoinduced O-H bond-breaking (Berto et al., 2016). Moreover,  $^3\text{VL}^*$  can initiate H-atom abstraction from the -CHO  
239 group of VL, generating ketyl radicals via Norrish-type reactions (Vione et al., 2019). Also, similar reactions can be initiated  
240 by  $\cdot\text{OH}$  (Gelencsér et al., 2003; Hoffer et al., 2004; Chang and Thompson, 2010; Sun et al., 2010), which in this study can be  
241 generated from the reaction between  $^3\text{VL}^*$  and  $\text{O}_2$ , as well as nitrate photolysis. Oligomers can then form via the coupling of  
242 phenoxy radicals or phenoxy and ketyl radicals (Sun et al., 2010; Berto et al., 2016; Vione et al., 2019). Absorbance increase  
243 at  $>350 \text{ nm}$  has also been reported for photosensitized oxidation of phenol and 4-phenoxyphenol (De Laurentiis et al., 2013a,  
244 2013b) and direct photolysis of tyrosine and 4-phenoxyphenol (Bianco et al., 2014) in which dimers have been identified as  
245 initial substrates. The continuous absorbance enhancement throughout 6 h of irradiation correlated with the observation of  
246 oligomers and nitrated compounds after irradiation. However, the increasing concentration of small organic acids (Fig. S5)  
247 throughout the experiments suggests that fragmentation, which results in the decomposition of initially formed oligomers  
248 and formation of smaller oxygenated products (Huang et al., 2018), is important at longer irradiation times. Overall, these  
249 trends establish that secondary oxidants from  $^3\text{VL}^*$  and  $\text{O}_2$  are necessary for the efficient formation of light-absorbing  
250 compounds from both  $\text{VL}^*$  and  $\text{VL}+\text{AN}$ .

### 251 3.1.2 Effect of pH

252 The reactivity of  $^3\text{C}^*$  (Smith et al., 2014, 2015, 2016), aromatic photonitration by nitrate (Machado and Boule, 1995;  
253 Dzengel et al., 1999; Vione et al., 2005; Minero et al., 2007), and N(III)-mediated VL photo-oxidation (Pang et al., 2019a)  
254 have been demonstrated to be pH-dependent. In this study, the effect of pH on VL photo-oxidation was investigated within  
255 the range of 2.5 to 5, corresponding to typical cloud (2-7) pH values (Pye et al., 2020). The decay rates for both  $\text{VL}^*$  and  
256  $\text{VL}+\text{AN}$  increased as pH decreased ( $\text{VL}^*$  and  $\text{VL}+\text{AN}$  at pH 2.5: 1.5 and 1.3 times faster than at pH 4, respectively) (Fig.





257 S3b). For VL\*, this pH trend indicates that <sup>3</sup>VL\* are more reactive in their protonated form, which is opposite to that  
258 reported for 0.005 mM VL (Smith et al., 2016), likely due to the concentration dependence of the relative reactivities of  
259 protonated and neutral forms of <sup>3</sup>VL\*. It has been reported that the quantum yield for direct VL photodegradation is higher at  
260 pH 5 than at pH 2 for 0.005 mM VL, but they are not statistically different for 0.03 mM VL (Smith et al., 2016). Also,  
261 increases in hydrogen ion concentration can enhance the formation of HO<sub>2</sub><sup>•</sup> and H<sub>2</sub>O<sub>2</sub> and in turn, <sup>•</sup>OH formation (Du et al.,  
262 2011). In addition to these pH influences on VL\*, the dependence of N(III) (NO<sub>2</sub><sup>-</sup> + HONO) speciation on solution acidity  
263 (Pang et al., 2019a) also contributed to the observed pH effects for VL+AN. At pH 3.3, half of N(III) exists as HONO  
264 (Fischer and Warneck, 1996; Pang et al., 2019a), which has a higher quantum yield for <sup>•</sup>OH formation than that of NO<sub>2</sub><sup>-</sup> in  
265 the near-UV region (Arakaki et al., 1999; Kim et al., 2014). The increased <sup>•</sup>OH formation rates as pH decreases can lead to  
266 faster VL decay (Pang et al., 2019a). Also, NO<sub>2</sub><sup>-</sup>/HONO can generate <sup>•</sup>NO<sub>2</sub> via oxidation by <sup>•</sup>OH (Reactions 4 and 15; Table  
267 1) (Pang et al., 2019a). As pH decreases, the higher reactivity of <sup>3</sup>VL\* and HONO being the dominant N(III) species can  
268 lead to faster VL photo-oxidation.

269 As pH decreased, the normalized abundance of products, particularly oligomers and functionalized monomers, was  
270 higher for both VL\* and VL+AN, further indicating that <sup>3</sup>VL\* are more reactive in their protonated form. The most  
271 abundant products observed were a substituted VL (C<sub>10</sub>H<sub>10</sub>O<sub>5</sub>) and VL dimer (C<sub>16</sub>H<sub>14</sub>O<sub>6</sub>; No. 5, Table S3) at pH 4 and pH  
272 <4, respectively (Figs. 1c-h). Furthermore, a tetramer was observed only in VL\* at pH 2.5. For VL+AN, the normalized  
273 abundance of nitrogen-containing compounds also increased at lower pH (Table S2), likely due to increased <sup>•</sup>OH and <sup>•</sup>NO<sub>2</sub>  
274 formation. The potential imidazole derivative (C<sub>3</sub>H<sub>5</sub>N<sub>3</sub>O<sub>2</sub>) was observed only at pH 4 possibly due to the pH dependence of  
275 ammonium speciation (pK<sub>a</sub> = 9.25). Imidazole formation requires the nucleophilic attack of ammonia on the carbonyl group  
276 (Yu et al., 2011), and at pH 4, the concentration of dissolved ammonia in VL+AN was about 10 or 30 times higher than that  
277 at pH 3 or pH 2.5, respectively. At different pH, the O:C and H:C ratios in VL\* and VL+AN had no significant differences  
278 (Figs. S7c-d and S9), but molecules with higher O:C ratios (>0.6) were more abundant at pH <4. Accordingly, the <OS<sub>c</sub>>  
279 pH <4 for both VL\* and VL+AN were higher than that at pH 4, consistent with higher <OS<sub>c</sub>> observed at pH 5 compared to  
280 pH 7 for the <sup>•</sup>OH-mediated photo-oxidation of syringol (Sun et al., 2010). Essentially, the higher reactivity of <sup>3</sup>VL\* and  
281 predominance of HONO over nitrite at lower pH result in increased formation of products mainly composed of oligomers  
282 and functionalized monomers.

283 The higher absorbance enhancement for both VL\* and VL+AN (Fig. 2b) as pH increased may be attributed to  
284 redshifts and increased visible light absorption of reaction products (Pang et al., 2019a). When a phenolic molecule  
285 deprotonates at higher pH, an ortho- or para- electron-withdrawing group, such as a nitro or aldehyde group, can attract a  
286 portion of the negative charge towards its oxygen atoms through induced and conjugated effects, leading to the extension of  
287 chromophore from the electron-donating group (e.g., -O<sup>-</sup>) to the electron-withdrawing group via the aromatic ring (Carey,  
288 2000; Williams and Fleming, 2008; Pang et al., 2019a). Hence, the delocalization of the negative charge in phenolates leads  
289 to significant redshifts (Mohr et al., 2013).



### 290 3.1.3 Effect of VOCs and inorganic anions

291 Aerosols are a complex mix of organic and inorganic compounds (Kanakidou et al., 2005). We explored the photo-oxidation  
292 behavior of VL, with and without nitrate, in the presence of VOCs (2-propanol, IPA) and inorganic anions (sodium  
293 bicarbonate, NaBC). For both VL\* and VL+AN, there was no significant change in VL decay (Figs. S3c-d), and comparable  
294 absorbance enhancements (Figs. 2c-d) were observed upon the addition of IPA and NaBC. However, the characterization of  
295 reaction products revealed the distinct effects of these compounds on the photo-oxidation of VL. Both IPA and NaBC  
296 increased the normalized abundance of products from VL\* (by a factor of 2.4 and 1.4, respectively) and VL+AN (by a factor  
297 of ~4) (Table S2). The major product observed in VL\*+IPA (Fig. S10a) was a dimer (C<sub>16</sub>H<sub>14</sub>O<sub>6</sub>). Also, higher oligomers up  
298 to tetramers (e.g., C<sub>31</sub>H<sub>22</sub>O<sub>12</sub>) not observed in VL\* were noted. A possible explanation may be the additional generation of  
299 <sup>•</sup>HO<sub>2</sub> from the reaction of IPA with <sup>•</sup>OH (Warneck and Wurzinger, 1988) (Reactions 16 and 17; Table 1), which can originate  
300 from <sup>3</sup>VL\* or nitrate photolysis, inducing reactions such as oxidation and nitration. As discussed earlier, <sup>•</sup>HO<sub>2</sub> can form  
301 H<sub>2</sub>O<sub>2</sub>, a photolytic source of <sup>•</sup>OH (Anastasio et al., 1996; Du et al., 2011). In the presence of IPA, the increase in normalized  
302 abundance of products (VL+AN+IPA: 3.8 times vs. VL\*+IPA: 2.4 times; Table S2) and <O<sub>s</sub>> (VL+AN+IPA: -0.13 to 0.08  
303 vs. VL\*+IPA: -0.16 to -0.10; Table S2) being more evident for VL+AN compared to VL\* also supports the potential  
304 importance of reactions involving <sup>•</sup>HO<sub>2</sub> and nitrate photolysis products such as the secondary photochemistry between  
305 <sup>•</sup>HO<sub>2</sub>/O<sub>2</sub><sup>•</sup>(<sub>aq</sub>) and photoproducted NO<sub>x</sub>(<sub>aq</sub>) enhancing HONO(<sub>g</sub>) production from nitrate photolysis in the presence of dissolved  
306 aliphatic organic matter (Wang et al., 2021) as discussed in Sect. 3.1.1. This chemistry may have operated in VL+AN+IPA  
307 considering that <sup>•</sup>HO<sub>2</sub>/O<sub>2</sub><sup>•</sup> may originate from multiple sources in this experiment: nitrate photolysis (Reaction 10; Table 1)  
308 (Jung et al., 2017; Wang et al., 2021), the reactions of <sup>3</sup>VL\* in the presence of O<sub>2</sub> (see Sect. 3.1), or reaction of IPA with <sup>•</sup>OH  
309 (Warneck and Wurzinger, 1988) (Reactions 16 and 17; Table 1). In other words, the role of nitrate in VL photo-oxidation is  
310 enhanced in the presence of IPA, likely due to additional <sup>•</sup>HO<sub>2</sub>/O<sub>2</sub><sup>•</sup> formation. In VL+AN+IPA, nitrate photolysis likely  
311 converted C<sub>16</sub>H<sub>14</sub>O<sub>6</sub> (from VL\*+IPA) to C<sub>15</sub>H<sub>12</sub>O<sub>8</sub> (Figs. S10a-b) via demethylation and then multiple hydroxylations.  
312 Nitrate photolysis generates <sup>•</sup>OH, and demethylation has been reported to be enhanced at high <sup>•</sup>OH exposure (Gold et al.,  
313 1983). Moreover, alcohols can affect the structure of water, causing a localized patterning or organization that changes the  
314 solvation environment, which can account for reactivity enhancement in the presence of alcohol-containing solvents (Berke  
315 et al., 2019). Berke et al. (2019) has demonstrated that IPA and other alcohols (e.g., ethanol) can promote the production of  
316 light-absorbing compounds, i.e., imidazoles, from the reactions between glyoxal and ammonium sulfate. This phenomenon  
317 has been attributed to the formation of micro-heterogeneities of hydrated alcohol molecules in a complex solution  
318 environment composed of solvated sulfate ions and a mixture of reactants and products upon the addition of alcohols. As  
319 proposed by an earlier study (Onori and Santucci, 1996), if the water in the SOA-mimicking solutions exists in two forms,  
320 bulk and hydrating, the micro-heterogeneities may interact with water/nitrate matrix to sequester the reactants and products,  
321 concentrating them within a smaller effective solvent volume and consequently resulting in increased normalized abundance  
322 of products (Berke et al., 2019).



323 For NaBC which does not produce  $\cdot\text{HO}_2$  upon reactions with  $\cdot\text{OH}$  under air-saturated conditions (Gen et al., 2019b),  
324 the increased normalized abundance of products may be due to other reactions promoted by the carbonate radical ( $\text{CO}_3^{\cdot-}$ ),  
325 which can be generated from the reactions of bicarbonate/carbonate with  $\cdot\text{OH}$  (Reactions 18 and 19; Table 1) (Neta et al.,  
326 1988; Wojnárovits et al., 2020) or  $^3\text{VL}^*$  (Reactions 20 and 21; Table 1) (Canonica et al., 2005).  $\text{CO}_3^{\cdot-}$  is a selective oxidant  
327 that reacts with organic molecules at a lower rate than  $\cdot\text{OH}$  and readily reacts with electron-rich parts of phenols, aromatic  
328 amines, and sulfur-containing compounds (e.g., glutathione) through both electron transfer and H-abstraction (Huang and  
329 Mabury, 2000; Wojnárovits et al., 2020). Similar to IPA, the enhancement of normalized abundance of products  
330 ( $\text{VL}+\text{AN}+\text{NaBC}$ : 4.3 times vs.  $\text{VL}^*+\text{NaBC}$ : 1.4 times; Table S2) and  $\langle\text{OS}_c\rangle$  ( $\text{VL}+\text{AN}+\text{NaBC}$ : -0.13 to 0.08 vs.  
331  $\text{VL}^*+\text{NaBC}$ : -0.16 to -0.11; Table S2) was more obvious for  $\text{VL}+\text{AN}+\text{NaBC}$  than  $\text{VL}^*+\text{NaBC}$ , further underlining the  
332 contributions of nitrate photolysis products. For example, it has been reported that carbonate and bicarbonate can  
333 substantially increase the photodegradation of electron-rich compounds (e.g., catechol) by nitrate (Vione et al., 2009).  
334 Bicarbonate can enhance the photolysis of nitrate via a solvent-cage effect, reacting with photolysis-derived  $\cdot\text{OH}$  before it  
335 escapes the surrounding cage of the water molecules. This prevents the recombination of  $\cdot\text{OH}$  and  $\cdot\text{NO}_2$  inside the solvent  
336 cage that otherwise would yield back  $\text{NO}_3^- + \text{H}^+$ , which reduces the quantum yield of  $\cdot\text{OH}$  photoproduction (Bouillon and  
337 Miller, 2005). This scavenging of in-cage  $\cdot\text{OH}$  by bicarbonate would then hinder recombination, resulting in a higher  
338 generation rate of  $\text{CO}_3^{\cdot-} + \cdot\text{OH}$  with bicarbonate compared to  $\cdot\text{OH}$  alone without bicarbonate. However, in our experiments,  
339 NaBC did not cause any substantial change in the decay of VL for both  $\text{VL}^*$  and  $\text{VL}+\text{AN}$ , although it promoted higher  
340 normalized abundance of products. The major product in  $\text{VL}^*+\text{NaBC}$  was a functionalized monomer ( $\text{C}_7\text{H}_4\text{O}_4$ ; No. 6, Table  
341 S3; Fig. S10c). Unlike  $\text{VL}^*+\text{IPA}$ , no tetramers were observed in  $\text{VL}^*+\text{NaBC}$ . Similar to  $\text{VL}+\text{AN}+\text{IPA}$ , the addition of  
342 NaBC to  $\text{VL}+\text{AN}$  resulted in trimers and a high-abundance dimer ( $\text{C}_{15}\text{H}_{12}\text{O}_8$ ; No. 7, Table S3) (Figs. S10b and S10d).  
343 Overall,  $\text{VL}+\text{AN}+\text{IPA}$  had more oligomers while  $\text{VL}+\text{AN}+\text{NaBC}$  had more functionalized monomers (e.g.,  $\text{C}_8\text{H}_6\text{O}_4$ ; No. 8,  
344 Table S3). These findings suggest that aside from low pH ( $<4$ ), the formation of oligomers from VL photo-oxidation can  
345 also be promoted by presence of VOCs and inorganic anions likely via the generation of radicals such as  $\cdot\text{HO}_2$  and  $\text{CO}_3^{\cdot-}$   
346 which can also interact with nitrate photolysis products.

347 The addition of IPA or NaBC to  $\text{VL}^*$  resulted in products with higher O:C and H:C ratios (Figs. S11a and S11c).  
348 Although the products were more abundant in  $\text{VL}^*+\text{IPA}$  than with NaBC, the distribution of their products in van Krevelen  
349 diagrams was rather similar. The increased in  $\langle\text{OS}_c\rangle$  in the presence of IPA or NaBC was more significant for  $\text{VL}+\text{AN}$  than  
350  $\text{VL}^*$ , likely due to the interactions of nitrate photolysis products with  $\cdot\text{HO}_2$  and  $\text{CO}_3^{\cdot-}$ . For  $\text{VL}+\text{AN}$ , IPA and NaBC also  
351 increased the O:C and H:C ratios (Figs. S11b and S11d), and most products had  $\text{OS}_c > 0$ , similar to less volatile and semi-  
352 volatile oxygenated organic aerosols (LV-OOA and SV-OOA) (Kroll et al., 2011).



### 353 3.1.4 Distribution of potential BrC compounds

354 Figure S12 plots the DBE values vs. number of carbons ( $n_c$ ) (Lin et al., 2018) for the 50 most abundant products from pH 4  
355 experiments under air-saturated conditions, along with reference to DBE values corresponding to fullerene-like  
356 hydrocarbons (Lobodin et al., 2012), cata-condensed polycyclic aromatic hydrocarbons (PAHs) (Siegmann and Sattler, 2000),  
357 and linear conjugated polyenes with a general formula  $C_xH_{x+2}$ . As light absorption by BrC requires uninterrupted conjugation  
358 across a significant part of the molecular structure, compounds with DBE/ $n_c$  ratios (shaded area in Fig. S12) greater than that  
359 of linear conjugated polyenes are potential BrC compounds (Lin et al., 2018). Based on this criterion and the observed  
360 absorbance enhancement at  $>350$  nm (Fig. 2), the majority of the 50 most abundant products from pH 4 experiments under  
361 air-saturated conditions were potential BrC chromophores composed of monomers and oligomers up to tetramers. However,  
362 as ESI-detected compounds in BB organic aerosols has been reported to be mainly molecules with  $n_c < 25$  (Lin et al., 2018),  
363 there may be higher oligomers that were not detected in our reaction systems.

### 364 3.2 Effect of reactants concentration and molar ratios on the aqueous photo-oxidation of vanillin

365 To examine the influence of VL and nitrate concentration and their molar ratios on VL photo-oxidation, we also  
366 characterized the reaction products from lower [VL] (0.01 mM VL\*; A14; Table S2), lower concentrations and an equal  
367 molar ratio of VL/nitrate (0.01 mM VL + 0.01 mM AN; A15; Table S2), and lower [VL] and 1:100 molar ratio of VL/nitrate  
368 (0.01 mM VL + 1 mM AN; A16; Table S2) at pH 4. The normalized abundance of products from low [VL] experiments  
369 (A14-A16; Table S2) were up to 1.4 times higher than that of high [VL] experiments (A5 and A7; Table S2). Nevertheless,  
370 the major products for both low and high [VL] experiments were functionalized monomers (Figs. 1c-d and S13a-c) such as  
371  $C_8H_6O_4$  and  $C_{10}H_{10}O_5$ . For both VL\* and VL+AN, the contribution of  $<200$  m/z to the normalized abundance of products  
372 was higher at low [VL] than at high [VL], while the opposite was observed for  $>300$  m/z (Fig. S13d). This indicates that  
373 functionalization was favored at low [VL], as supported by the higher  $\langle OS_c \rangle$ , while oligomerization was the dominant  
374 pathway at high [VL], consistent with more oligomers or polymeric products reported from high phenols concentration (e.g.,  
375 0.1 to 3 mM) (Li et al., 2014; Slikboer et al., 2015; Ye et al., 2019). A possible explanation is that at 1:1 VL/nitrate, VL  
376 efficiently competes with  $NO_2^-$  for  $\cdot OH$  (from nitrate or nitrite photolysis, Reaction 4; Table 1) and indirectly reduces  $\cdot NO_2$ .  
377 Similarly, hydroxylation has been suggested to be an important pathway for 1:1 VL/nitrite than in 1:10 VL/nitrite (Pang et  
378 al., 2019a). This may also be the reason why 1:1 VL/nitrate (A15; Table S2) had higher  $\langle OS_c \rangle$  than 1:100 (A16; Table S2)  
379 VL/nitrate but had fewer N-containing compounds compared to the latter. Moreover, the contribution of  $<200$  m/z to the  
380 normalized abundance of products was higher for 1:1 than 1:100 VL/nitrate molar ratio, further suggesting the formation of  
381 more oxidized products.



### 382 3.3 Participation of ammonium in the aqueous photo-oxidation of vanillin

383 Imidazole and imidazole derivatives have been reported to be the major products of glyoxal and ammonium sulfate reactions  
384 at pH 4 (Galloway et al., 2009; Yu et al., 2011; Sedehi et al., 2013; Gen et al., 2018; Mabato et al., 2019). Here, we  
385 compared VL+AN and VL+SN at pH 4 in terms of reaction products and oxidative characteristics to confirm the  
386 participation of ammonium in the aqueous photo-oxidation of VL. In both experiments, the normalized abundance of the  
387 products was comparable (A7 and A13; Table S2), with C<sub>10</sub>H<sub>10</sub>O<sub>5</sub> as the most abundant product (Figs. 1d and S6a), but in  
388 VL+SN, there was a significant amount of a VL dimer (C<sub>15</sub>H<sub>12</sub>O<sub>8</sub>; No. 9, Table S3). Moreover, the nitrogen-containing  
389 compounds were distinct. Aside from the potential imidazole derivative (C<sub>5</sub>H<sub>5</sub>N<sub>3</sub>O<sub>2</sub>; No. 10, Table S3), C<sub>8</sub>H<sub>9</sub>NO<sub>3</sub> was also  
390 observed from VL+AN but only under N<sub>2</sub>-saturated conditions (Fig. 1b), probably due to further oxidation by secondary  
391 oxidants from <sup>3</sup>VL\*. The product analysis suggests the participation of ammonium in the aqueous-phase reactions.  
392 Ammonium salts are an important constituent of atmospheric aerosols particles (Jimenez et al., 2009), and reactions between  
393 dicarbonyls (e.g., glyoxal) and ammonia or primary amines have been demonstrated to form BrC (De Haan et al., 2009, 2011;  
394 Nozière et al., 2009; Shapiro et al., 2009; Lee et al., 2013; Powelson et al., 2014; Gen et al., 2018; Mabato et al., 2019).  
395 Relative to VL+AN, the products from VL+SN had higher O:C ratios (e.g., C<sub>7</sub>H<sub>4</sub>N<sub>2</sub>O<sub>7</sub>; No. 11, Table S3), OS<sub>c</sub>, and <OS<sub>c</sub>>  
396 values (Table S2).

### 397 3.4 Oxidation of guaiacol by photosensitized reactions of vanillin and photolysis of nitrate

398 The oxidation of phenols by <sup>3</sup>C\* has been mainly studied using non-phenolic aromatic carbonyls (Anastasio et al., 1996;  
399 Smith et al., 2014, 2015; Yu et al., 2014; Chen et al., 2020) and aromatic ketones (Canonica et al., 2000) as triplet precursors.  
400 Recently, <sup>3</sup>VL\* have also been shown to oxidize syringol (Smith et al., 2016), a non-carbonyl phenol, although the reaction  
401 products remain unknown. In this section, we discussed the photo-oxidation of guaiacol (GUA), a lignocellulosic BB  
402 pollutant (Kroftlić et al., 2015) that is also a non-carbonyl phenol, in the presence of VL (GUA+VL) or nitrate (GUA+AN).  
403 The dark experiments did not show any substantial loss of VL or GUA (Fig. S3e). Due to its poor light absorption in the  
404 solar range, GUA is not an effective photosensitizer (Smith et al., 2014; Yu et al., 2014). Accordingly, the direct GUA  
405 photodegradation resulted in minimal decay, which plateaued after ~3 hours. However, in the presence of VL or nitrate, the  
406 GUA decay was faster by 2.2 (GUA+VL) and 1.2 (GUA+AN) times, respectively, than for direct GUA photodegradation.  
407 This enhanced GUA decay rate may be due to the following main reactions: oxidation of GUA by <sup>3</sup>VL\* (or the secondary  
408 oxidants it generates upon reaction with O<sub>2</sub>), oxidation by <sup>•</sup>OH produced from nitrate photolysis, or nitration by <sup>•</sup>NO<sub>2</sub> from  
409 nitrate photolysis. As mentioned earlier, the <sup>3</sup>VL\* chemistry appears to be more important than that of nitrate photolysis  
410 even at 1:10 molar ratio of VL/nitrate on account of the much higher molar absorptivity of VL compared to that of nitrate  
411 (Fig. S1) and the high VL concentration (0.1 mM) used in this study. The decay of VL in GUA+VL (A18; Table S2) was 3  
412 times slower than that of VL\* (A5; Table S2), which may be due to competition between ground-state VL and GUA for  
413 reactions with <sup>3</sup>VL\* (or the secondary oxidants it generates upon reaction with O<sub>2</sub>) or increased conversion of <sup>3</sup>VL\* back to



414 the ground state through the oxidation of GUA (Anastasio et al., 1996; Smith et al., 2014). The corresponding absorbance  
415 changes for the GUA experiments (Fig. 1e) were consistent with the observed decay trends. The minimal absorbance  
416 changes for the direct GUA photodegradation also plateaued after ~3 hours. Moreover, the difference between GUA photo-  
417 oxidation in the presence of VL or nitrate was more evident, with the former showing much higher absorbance enhancement.  
418 Similarly, Yang et al. (2021) also observed greater light absorption during nitrate-mediated photo-oxidation relative to direct  
419 GUA photodegradation.

420 For the direct GUA photodegradation, GUA+VL, and GUA+AN, the normalized abundance of products was  
421 calculated only for GUA+VL (2.2; Table S2), as the GUA signal from the UHPLC-qToF-MS in the positive ion mode was  
422 weak, which may introduce large uncertainties during normalization. Nonetheless, the number of products detected from  
423 these experiments (178, 266, and 844 for the direct GUA photodegradation, GUA+AN, and GUA+VL, respectively)  
424 corroborates the kinetics and absorbance results. The major products (Fig. 3a) from the direct photodegradation of GUA  
425 were  $C_{14}H_{14}O_4$  (No. 19, Table S3), a typical GUA dimer, and a trimer ( $C_{21}H_{20}O_6$ ; No. 20, Table S3) which likely originated  
426 from photoinduced O-H bond-breaking (Berto et al., 2016). In general, higher absolute signal areas was noted for oligomers  
427 (e.g.,  $C_{14}H_{14}O_4$ ,  $C_{21}H_{20}O_6$ ) and hydroxylated products (e.g.,  $C_7H_8O_4$ ) in both GUA+VL and GUA+AN, similar to those  
428 observed from GUA oxidation by triplets of 3,4-dimethoxybenzaldehyde (DMB; a non-phenolic aromatic carbonyl) or  $\cdot OH$   
429 (from  $H_2O_2$  photolysis) (Yu et al., 2014). In contrast to the GUA aqSOA reported by Yu et al. (2014), the photo-oxidation of  
430 GUA in this study yielded nitrated compounds (e.g.,  $C_9H_{14}N_2O_6$ ,  $C_{11}H_{14}N_2O_9$ ) from GUA+AN and VL dimers (e.g.,  
431  $C_{16}H_{12}O_6$ ) from GUA+VL. However, based on a recent work on the aqueous photo-oxidation of guaiacyl acetone (another  
432 aromatic phenolic carbonyl) by DMB triplets, the hydroxylation and dimerization of DMB can also contribute to aqSOA  
433 (Jiang et al., 2021). The contributions from DMB-participated reactions were only minor due to the low initial DMB  
434 concentration (0.005 mM). Relative to GUA+AN, higher signals for dimers such as  $C_{14}H_{14}O_4$  and  $C_{16}H_{12}O_6$  were noted in  
435 GUA+VL, possibly due to both GUA and ground-state VL being available as oxidizable substrates for  $^3VL^*$  and the  
436 secondary oxidants it can generate. Also, a potential GUA tetramer ( $C_{28}H_{24}O_8$ , No. 21, Table S3) was observed only in  
437 GUA+VL, consistent with higher oligomer formation from the triplets-mediated photo-oxidation of phenolics relative to  
438  $\cdot OH$ -assisted photo-oxidation (Yu et al., 2014). In general, the products from the direct GUA photodegradation, GUA+VL,  
439 and GUA+AN had similar  $OS_c$  values (-0.5 to 0.5) (Figs. 3b-d), falling into the criterion of BBOA and SV-OOA (Kroll et  
440 al., 2011). In this work, efficient GUA photo-oxidation was observed in the presence of VL and AN, forming aqSOA  
441 composed of oligomers, hydroxylated products, and nitrated compounds (for GUA+AN). The higher product signals from  
442 GUA+VL compared to GUA+AN is likely due to the availability of both GUA and ground-state VL as aqSOA precursors.

### 443 3.5 Photo-oxidation pathways of vanillin via direct photosensitization and in the presence of nitrate

444 The most probable pathways of direct photosensitized and nitrate-mediated photo-oxidation of VL were proposed (Fig. 4). In  
445 Scheme 1 (pH 4 and pH <4 under air-saturated conditions),  $^3VL^*$  and  $\cdot OH$  (from  $^3VL^*$  or nitrate photolysis) can initiate H-





446 atom abstraction to generate phenoxy or ketyl radicals (Huang et al., 2018; Vione et al., 2019). At pH 4, ring-opening  
447 products (Fig. S5) from fragmentation in both VL\* and VL+AN may have reacted with VL or dissolved ammonia to  
448 generate C<sub>10</sub>H<sub>10</sub>O<sub>5</sub> (Pang et al., 2019b) and a potential imidazole derivative (C<sub>5</sub>H<sub>5</sub>N<sub>3</sub>O<sub>2</sub>), respectively. Moreover, nitrate  
449 photolysis products promoted functionalization and nitration (e.g., C<sub>16</sub>H<sub>10</sub>N<sub>2</sub>O<sub>9</sub>). At pH <4, the reactivity of <sup>3</sup>VL\* increased  
450 as suggested by the abundance of oligomers (e.g., C<sub>16</sub>H<sub>14</sub>O<sub>6</sub>) and increased normalized abundance of N-containing  
451 compounds.

452 In Scheme 2 (pH 4, IPA or NaBC, under air-saturated conditions), additional radicals generated (<sup>•</sup>HO<sub>2</sub> and CO<sub>3</sub><sup>•-</sup>)  
453 likely promoted more reactions. An abundant dimer (C<sub>16</sub>H<sub>14</sub>O<sub>6</sub>) and higher oligomers (e.g., tetramers, C<sub>31</sub>H<sub>22</sub>O<sub>12</sub>) were  
454 identified in VL\*+IPA, possibly due to <sup>•</sup>HO<sub>2</sub>-initiated reactions, while a functionalized monomer (C<sub>7</sub>H<sub>4</sub>O<sub>4</sub>) was abundant in  
455 VL\*+NaBC. In general, nitrate enhanced both oligomerization and functionalization in VL+IPA or VL+NaBC. In  
456 VL+AN+IPA, C<sub>15</sub>H<sub>12</sub>O<sub>8</sub> likely originated from C<sub>16</sub>H<sub>14</sub>O<sub>6</sub> via demethylation and multiple hydroxylations. In VL+AN+NaBC,  
457 C<sub>8</sub>H<sub>6</sub>O<sub>4</sub> was possibly generated via H-atom abstraction from -OCH<sub>3</sub> by <sup>•</sup>OH, and further addition with O<sub>2</sub> is energy  
458 barrierless (Priya and Lakshmi pathi, 2017; Sun et al., 2019), generating a hydroperoxide (-OCH<sub>2</sub>OOH) that readily  
459 decompose to form -OCH<sub>2</sub>O<sup>•</sup> and <sup>•</sup>OH (Yaremenko et al., 2016). -OCH<sub>2</sub>O<sup>•</sup> is finally transformed into -OCHO with the  
460 elimination of HO<sub>2</sub> in the presence of O<sub>2</sub> (Sun et al., 2019). Moreover, the abundance of C<sub>15</sub>H<sub>12</sub>O<sub>8</sub> was higher in  
461 VL+AN+NaBC than in VL\*+NaBC.

#### 462 4 Conclusions and atmospheric implications

463 This study shows that the photo-oxidation of VL via its direct photosensitized reactions and in the presence of nitrate can  
464 generate aqSOA composed of oligomers, functionalized monomers, oxygenated ring-opening products, and nitrated  
465 compounds (for nitrate-mediated reactions). The characterization of products presented in this work complements earlier  
466 studies (e.g., Smith et al. 2014, 2015, 2016) that mainly discussed the kinetics and aqSOA yield of triplet-driven oxidation of  
467 phenols. Although nitrate did not substantially affect the VL decay rates, likely due to much higher molar absorptivity of VL  
468 than nitrate and high VL concentration used in this work, the presence of nitrate promoted functionalization and nitration,  
469 indicating the significance of nitrate photolysis in this aqSOA formation pathway. While nitration can be an important  
470 process for producing light-absorbing organics or BrC (Jacobson, 1999; Kahnt et al., 2013; Mohr et al., 2013; Laskin et al.,  
471 2015; Teich et al., 2017; Li et al., 2020), its effect on triplet-generating aromatics has not yet been examined in detail. On a  
472 related note, a recent work (Ma et al., 2021) mimicking phenol oxidation by DMB (a non-phenolic aromatic carbonyl)  
473 triplets in more concentrated conditions in aerosol liquid water (ALW) showed that significantly higher AN concentration  
474 (0.5 M) increased the photodegradation rate constant for guaiacyl acetone (an aromatic phenolic carbonyl with high Henry's  
475 law constant, 1.2 × 10<sup>6</sup> M atm<sup>-1</sup>; McFall et al., 2020) by >20 times which was ascribed to <sup>•</sup>OH formation from nitrate  
476 photolysis (Brezonik and Fulkerson-Brekken, 1998; Chu and Anastasio, 2003). The same study also estimated that reactions  
477 of phenols with high Henry's law constants (10<sup>6</sup> to 10<sup>9</sup> M atm<sup>-1</sup>) can be important for SOA formation in ALW, with



478 mechanisms mainly governed by  $^3\text{C}^*$  and  $^1\text{O}_2$  (Ma et al., 2021). Likewise, Zhou et al. (2019) reported that the direct  
479 photodegradation of acetosyringone was faster by about 6 times in the presence of 2 M  $\text{NaClO}_4$ . However, the opposite was  
480 noted for the photodegradation of VL in sodium sulfate or sodium nitrate, which would occur slower (2 times slower in 0.5  
481 M sodium sulfate and ~10 times slower in 0.124 M sodium nitrate) in ALW relative to dilute aqueous phase in clouds. These  
482 suggest that the nature of inorganic ions may have an essential role in the photodegradation of organic compounds in the  
483 aqueous phase (Loisel et al., 2021).

484 Furthermore, a potential imidazole derivative observed from the VL+AN (A7; Table S2) experiment suggests that  
485 ammonium may participate in aqSOA formation from the photo-oxidation of phenolic aromatic carbonyls. Also, the  
486 oligomers from these reaction systems may be rather recalcitrant to fragmentation based on their high abundance, even at the  
487 longest irradiation time used in this study. Nonetheless, the increasing concentration of small organic acids over time implies  
488 that fragmentation becomes important at extended irradiation times. Aromatic carbonyls and nitrophenols have been reported  
489 to be the most important classes of BrC in cloud water heavily affected by biomass burning in the North China Plain  
490 (Desyaterik et al., 2013). Correspondingly, the most abundant products from our reaction systems (pH 4, air-saturated  
491 solutions) are mainly potential BrC chromophores. These suggest that aqSOA generated in cloud/fog water from the  
492 oxidation of biomass burning aerosols via direct photosensitized reactions and nitrate photolysis products can impact aerosol  
493 optical properties and radiative forcing, particularly for areas where biomass burning is intensive.

494 Our results indicate that the photo-oxidation of VL is influenced by secondary oxidants from VL triplets, pH, the  
495 presence of VOCs and inorganic anions, and reactants concentration and molar ratios. Compared to  $\text{N}_2$ -saturated conditions,  
496 more efficient VL photo-oxidation was observed under air-saturated conditions ( $\text{O}_2$  is present), which can be attributed to the  
497 generation of secondary oxidants (e.g.,  $^1\text{O}_2$ ,  $\text{O}_2^{\cdot-}/\text{HO}_2$ ,  $\cdot\text{OH}$ ) from  $^3\text{VL}^*$ . Further enhancement of VL photo-oxidation under  
498 air-saturated conditions in the presence of nitrate indicates synergistic effects between secondary oxidants from VL triplets  
499 and nitrate photolysis products. Additionally, the formation of oligomers from VL photo-oxidation was observed to be  
500 promoted at low pH (<4) or in the presence of IPA/NaBC, which likely generated additional radicals such as  $\cdot\text{HO}_2$  and  $\text{CO}_3^{\cdot-}$ .  
501 As aerosols comprise more complex mixtures of organic and inorganic compounds, it is worthwhile to explore the impacts  
502 of other potential aerosol constituents on aqSOA formation and photo-oxidation studies. This can also be beneficial in  
503 understanding the interplay among different reaction mechanisms during photo-oxidation. Low VL concentration favored  
504 functionalization, while oligomerization prevailed at high VL concentration, consistent with past works (Li et al., 2014;  
505 Slikboer et al., 2015; Ye et al., 2019). Hydroxylation was observed to be important for equal molar ratios of VL and nitrate,  
506 likely due to VL competing with nitrite for  $\cdot\text{OH}$ . The oxidation of guaiacol, a non-carbonyl phenol, by photosensitized  
507 reactions of vanillin was also shown to be more efficient than that by nitrate photolysis products.

508 In this study, we investigated reactions of VL and nitrate at concentrations in cloud/fog water. The concentrations of  
509 VL and nitrate can be significantly higher in aqueous aerosol particles. As a major component of aerosols, the concentration  
510 of nitrate can be as high as sulfate (Huang et al., 2014). More studies should then explore the direct photosensitized  
511 oxidation and nitrate-mediated photo-oxidation of other biomass burning-derived phenolic aromatic carbonyls, particularly



512 those with high molar absorption coefficients and can generate  $^3\text{C}^*$ . The influences of reaction conditions should also be  
513 investigated to better understand the oxidation pathways. Considering that biomass burning emissions are expected to  
514 increase continuously, further studies on these aqSOA formation pathways are strongly suggested.

515

516 *Data availability.*

517 The data used in this publication are available to the community and can be accessed by request to the corresponding author.

518 *Author contributions.*

519 BRG designed and conducted the experiments; YL provided assistance in measurements and helped to analyze  
520 experimental data; YJ provided assistance in measurements; BRG, YL, and CKC wrote the paper. All co-authors  
521 contributed to the discussion of the manuscript.

522 *Competing interests.*

523 The authors declare that they have no conflict of interest.

524 *Acknowledgments.*

525 This work was financially supported by the National Natural Science Foundation of China (41875142 and 42075100).  
526 D.D.H. acknowledges support from the National Natural Science Foundation of China (21806108). X.L. acknowledges  
527 support from the Local Innovative and Research Teams Project of Guangdong Pearl River Talents Program  
528 (2019BT02Z546). T.N. acknowledges support from the Hong Kong Research Grants Council (21304919) and City  
529 University of Hong Kong (9610409). C.H.L. acknowledges support from the City University of Hong Kong (9610458 and  
530 7005576).

## 531 **References**

532 Abida, O., Mielke, L. H., and Osthoff, H. D.: Observation of gas-phase peroxyxynitrous and peroxyxynitric acid during the  
533 photolysis of nitrate in acidified frozen solutions, *Chem. Phys. Lett.*, 511, 187–192,  
534 <https://doi.org/10.1016/j.cplett.2011.06.055>, 2011.

535

536 Anastasio, C., Faust, B. C., and Rao, C. J.: Aromatic carbonyl compounds as aqueous-phase photochemical sources of  
537 hydrogen peroxide in acidic sulfate aerosols, fogs, and clouds. 1. Non-phenolic methoxybenzaldehydes and  
538 methoxyacetophenones with reductants (phenols), *Environ. Sci. Technol.*, 31, 218–232, <https://doi.org/10.1021/es960359g>,  
539 1996.

540

541 Arakaki, T., Miyake, T., Hirakawa, T., and Sakugawa, H.: pH dependent photoformation of hydroxyl radical and absorbance  
542 of aqueous-phase N(III) ( $\text{HNO}_2$  and  $\text{NO}_2^-$ ), *Environ. Sci. Technol.*, 33, 2561–2565, <https://doi.org/10.1021/es980762i>, 1999.

543

544 Bateman, A. P., Laskin, J., Laskin, A., and Nizkorodov, S. A.: Applications of high-resolution electrospray ionization mass  
545 spectrometry to measurements of average oxygen to carbon ratios in secondary organic aerosols, *Environ. Sci. Technol.*, 46,  
546 8315–8324, <https://doi.org/10.1021/es3017254>, 2012.



- 547 Berke, A. E., Bhat, T. A., Myers, H., Gubbins, E. F., Nwankwo, A. A. O., Lu, K., Timpane, L., and Keller, C.: Effect of  
548 short-chain alcohols on the bulk-phase reaction between glyoxal and ammonium sulfate, *Atmos. Environ.*, 198, 407–416,  
549 <https://doi.org/10.1016/j.atmosenv.2018.11.015>, 2019.
- 550
- 551 Berto, S., De Laurentiis, E., Tota, T., Chiavazza, E., Daniele, P.G., Minella, M., Isaia, M., Brigante, M., and Vione, D.:  
552 Properties of the humic-like material arising from the photo-transformation of L-tyrosine, *Sci. Total Environ.*, 434–444,  
553 <https://doi.org/10.1016/j.scitotenv.2015.12.047>, 2016.
- 554
- 555 Bianco, A., Minella, M., De Laurentiis, E., Maurino, V., Minero, C., and Vione, D.: Photochemical generation of  
556 photoactive compounds with fulvic-like and humic-like fluorescence in aqueous solution, *Chemosphere*, 111, 529–536,  
557 <https://doi.org/10.1016/j.chemosphere.2014.04.035>, 2014.
- 558
- 559 Bianco, A., Deguillaume, L., Vätilingom, M., Nicol, E., Baray, J.-L., Chaumerliac, N., and Bridoux, M.: Chemical  
560 characterization of cloud water collected at Puy de Dôme by FT-ICR MS reveals the presence of SOA components, *Environ.*  
561 *Sci. Technol.*, 52, 10275–10285, <https://doi.org/10.1021/acsearthspacechem.9b00153>, 2018.
- 562
- 563 Bianco, A., Passananti, M., Brigante, M., and Mailhot, G.: Photochemistry of the cloud aqueous phase: a review, *Molecules*,  
564 25, 423, <https://doi.org/10.3390/molecules25020423>, 2020.
- 565
- 566 Blando, J. D. and Turpin, B. J.: Secondary organic aerosol formation in cloud and fog droplets: a literature evaluation of  
567 plausibility, *Atmos. Environ.*, 34, 1623–1632, [https://doi.org/10.1016/S1352-2310\(99\)00392-1](https://doi.org/10.1016/S1352-2310(99)00392-1), 2000.
- 568
- 569 Bond, T. C., Streets, D. G., Yarber, K. F., Nelson, S. M., Woo, J.-H., and Klimont, Z.: A technology-based global inventory  
570 of black and organic carbon emissions from combustion, *J. Geophys. Res.*, 109, <https://doi.org/10.1029/2003JD003697>,  
571 2004.
- 572
- 573 Bouillon, R.C. and Miller, W.L.: Photodegradation of dimethyl sulfide (DMS) in natural waters: laboratory assessment of the  
574 nitrate-photolysis-induced DMS oxidation, *Environ. Sci. Technol.*, 39, 9471–9477, <https://doi.org/10.1021/es048022z>, 2005.
- 575
- 576 Brezonik, P. L. and Fulkerson-Brekken, J.: Nitrate-induced photolysis in natural waters: controls on concentrations of  
577 hydroxyl radical photo-intermediates by natural scavenging agents, *Environ. Sci. Technol.*, 32, 3004–3010,  
578 <https://doi.org/10.1021/es9802908>, 1998.
- 579
- 580 Canonica, S., Jans, U., Stemmler, K., and Hoigne, J.: Transformation kinetics of phenols in water: Photosensitization by  
581 dissolved natural organic material and aromatic ketones, *Environ. Sci. Technol.*, 29, 1822–1831,  
582 <https://doi.org/10.1021/es00007a020>, 1995.
- 583
- 584 Canonica, S., Hellrung, B., and Wirz, J.: Oxidation of phenols by triplet aromatic ketones in aqueous solution, *J. Phys.*  
585 *Chem.*, 104, 1226–1232, <https://doi.org/10.1021/jp9930550>, 2000.
- 586
- 587 Canonica, S., Kohn, T., Mac, M., Real, F.J., Wirz, J., and Von Gunten, U.: Photosensitizer method to determine rate  
588 constants for the reaction of carbonate radical with organic compounds, *Environ. Sci. Technol.*, 39, 9182–9188,  
589 <https://doi.org/10.1021/es051236b>, 2005.
- 590
- 591 Carey, F. A.: *Organic Chemistry*, 4th Ed., McGraw-Hill, USA, 2000.
- 592
- 593 Chang, J. L. and Thompson, J. E.: Characterization of colored products formed during irradiation of aqueous solutions  
594 containing H<sub>2</sub>O<sub>2</sub> and phenolic compounds, *Atmos. Environ.*, 44, 541–551, <https://doi.org/10.1016/j.atmosenv.2009.10.042>,  
595 2010.



- 596 Chen, Y., Li, N., Li, X., Tao, Y., Luo, S., Zhao, Z., Ma, S., Huang, H., Chen, Y., Ye, Z., and Ge, X.: Secondary organic  
597 aerosol formation from  $^3\text{C}^*$ -initiated oxidation of 4-ethylguaiaicol in atmospheric aqueous-phase, *Sci. Total Environ.*, 723,  
598 137953, <https://doi.org/10.1016/j.scitotenv.2020.137953>, 2020.  
599
- 600 Chu, L. and Anastasio, C.: Quantum yields of hydroxyl radical and nitrogen dioxide from the photolysis of nitrate on ice, *J.*  
601 *Phys. Chem. A*, 107, 9594–9602, <https://doi.org/10.1021/jp0349132>, 2003.  
602
- 603 Collett, J. L. Jr., Hoag, K. J., Sherman, D. E., Bator, A., and Richards, L. W.: Spatial and temporal variations in San Joaquin  
604 Valley fog chemistry, *Atmos. Environ.*, 33, 129–140, [https://doi.org/10.1016/S1352-2310\(98\)00136-8](https://doi.org/10.1016/S1352-2310(98)00136-8), 1998.  
605
- 606 Collett, J. L. Jr., Hoag, K. J., Rao, X., and Pandis, S. N.: Internal acid buffering in San Joaquin Valley fog drops and its  
607 influence on aerosol processing, *Atmos. Environ.*, 33, 4833–4847, [https://doi.org/10.1016/S1352-2310\(99\)00221-6](https://doi.org/10.1016/S1352-2310(99)00221-6), 1999.  
608
- 609 De Gouw, J. and Jimenez, J. L.: Organic aerosols in the Earth’s atmosphere, *Environ. Sci. Technol.*, 43, 7614–7618,  
610 <https://doi.org/10.1021/es9006004>, 2009.  
611
- 612 De Haan, D. O., Corrigan, A. L., Tolbert, M. A., Jimenez, J. L., Wood, S. E., and Turley, J. J.: Secondary organic aerosol  
613 formation by self-reactions of methylglyoxal and glyoxal in evaporating droplets, *Environ. Sci. Technol.*, 43, 8184–8190,  
614 <https://doi.org/10.1021/es902152t>, 2009.  
615
- 616 De Haan, D. O., Hawkins, L. N., Kononenko, J. A., Turley, J. J., Corrigan, A. L., Tolbert, M. A., and Jimenez, J. L.:  
617 Formation of nitrogen-containing oligomers by methylglyoxal and amines in simulated evaporating cloud droplets, *Environ.*  
618 *Sci. Technol.*, 45, 984–991, <https://doi.org/10.1021/es102933x>, 2011.  
619
- 620 De Haan, D.O., Pajunoja, A., Hawkins, L. N., Welsh, H.G., Jimenez, N. G., De Loera, A., Zauscher, M., Andretta, A. D.,  
621 Joyce, B. W., De Haan, A. C., Riva, M., Cui, T., Surratt, J. D., Cazaunau, M., Formenti, P., Gratien, A., Pangui, E., and  
622 Doussin, J-F.: Methylamine’s effects on methylglyoxal-containing aerosol: chemical, physical, and optical changes, *ACS*  
623 *Earth Space Chem.*, 3, 1706–1716, <https://doi.org/10.1021/acsearthspacechem.9b00103>, 2019.  
624
- 625 De Laurentiis, E., Socorro, J., Vione, D., Quivet, E., Brigante, M., Mailhot, G., Wortham, H., and Gligorovski, S.:  
626 Phototransformation of 4-phenoxyphenol sensitised by 4-carboxybenzophenone: Evidence of new photochemical pathways  
627 in the bulk aqueous phase and on the surface of aerosol deliquescent particles, *Atmos. Environ.*, 81, 569–578,  
628 <https://doi.org/10.1016/j.atmosenv.2013.09.036>, 2013a.  
629
- 630 De Laurentiis, E., Sur, B., Pazzi, M., Maurino, V., Minero, C., Mailhot, G., Brigante, M., and Vione, D.: Phenol  
631 transformation and dimerisation, photosensitised by the triplet state of 1-nitronaphthalene: A possible pathway to humic-like  
632 substances (HULIS) in atmospheric waters, *Atmos. Environ.*, 70, 318–327, <https://doi.org/10.1016/j.atmosenv.2013.01.014>,  
633 2013b.  
634
- 635 Desyaterik, Y., Sun, Y., Shen, X., Lee, T., Wang, X., Wang, T., and Collett, J. L. Jr.: Speciation of “brown” carbon in cloud  
636 water impacted by agricultural biomass burning in eastern China, *J. Geophys. Res. Atmos.*, 118, 7389–7399,  
637 <https://doi.org/10.1002/jgrd.50561>, 2013.  
638
- 639 Du, Y., Fu, Q. S., Li, Y., and Su, Y.: Photodecomposition of 4-chlorophenol by reactive oxygen species in UV/air system, *J.*  
640 *Hazard. Mater.*, 186, 491–496, <https://doi.org/10.1016/j.jhazmat.2010.11.023>, 2011.  
641
- 642 Dzengel, J., Theurich, J., and Bahnemann, D. W.: Formation of nitroaromatic compounds in advanced oxidation processes:  
643 photolysis versus photocatalysis, *Environ. Sci. Technol.*, 33, 294–300, <https://doi.org/10.1021/es980358j>, 1999.



- 644 Ervens, B., Turpin, B. J., and Weber, R. J.: Secondary organic aerosol formation in cloud droplets and aqueous particles  
645 (aqSOA): a review of laboratory, field and model studies, *Atmos. Chem. Phys.*, 11, 11069–11102,  
646 <https://doi.org/10.5194/acp-11-11069-2011>, 2011.
- 647
- 648 Fischer, M. and Warneck, P.: Photodecomposition of nitrite and undissociated nitrous acid in aqueous solution, *J. Phys.*  
649 *Chem.*, 100, 18749–18756, <https://doi.org/10.1021/jp961692+>, 1996.
- 650
- 651 Foote, C.S.: Definition of type I and type II photosensitized oxidation, *Photochem. Photobiol.*, 54, 659,  
652 <https://doi.org/10.1111/j.1751-1097.1991.tb02071.x>, 1991.
- 653
- 654 Galloway, M. M., Chhabra, P. S., Chan, A. W. H., Surratt, J. D., Flagan, R. C., Seinfeld, J. H., and Keutsch, F. N.: Glyoxal  
655 uptake on ammonium sulphate seed aerosol: reaction products and reversibility of uptake under dark and irradiated  
656 conditions, *Atmos. Chem. Phys.*, 9, 3331–3345, <https://doi.org/10.5194/acp-9-3331-2009>, 2009.
- 657
- 658 Gelencsér, A., Hoffer, A., Kiss, G., Tombácz, E., Kurdi, R., and Bencze, L.: In-situ formation of light-absorbing organic  
659 matter in cloud water, *J. Atmos. Chem.*, 45, 25–33, <https://doi.org/10.1023/A:1024060428172>, 2003.
- 660
- 661 Gen, M., Huang, D. D., and Chan, C. K.: Reactive uptake of glyoxal by ammonium-containing salt particles as a function of  
662 relative humidity, *Environ. Sci. Technol.*, 52, 6903–6911, <https://doi.org/10.1021/acs.est.8b00606>, 2018.
- 663
- 664 Gen, M., Zhang, R., Huang, D. D., Li, Y., and Chan, C. K.: Heterogeneous SO<sub>2</sub> oxidation in sulfate formation by photolysis  
665 of particulate nitrate, *Environ. Sci. Technol. Lett.*, 6, 86–91, <https://doi.org/10.1021/acs.estlett.8b00681>, 2019a.
- 666
- 667 Gen, M., Zhang, R., Huang, D. D., Li, Y., and Chan, C. K.: Heterogeneous oxidation of SO<sub>2</sub> in sulfate production during  
668 nitrate photolysis at 300 nm: Effect of pH, relative humidity, irradiation intensity, and the presence of organic compounds,  
669 *Environ. Sci. Technol.*, 53, 8757–8766, <https://doi.org/10.1021/acs.est.9b01623>, 2019b
- 670
- 671 George, C., Ammann, M., D’Anna, B., Donaldson, D.J., and Nizkorodov, S.A.: Heterogeneous photochemistry in the  
672 atmosphere, *Chem. Rev.*, 115, 4218–4258, <https://doi.org/10.1021/cr500648z>, 2015.
- 673
- 674 Gilardoni, S., Massoli, P., Paglione, M., Giulianelli, L., Carbone, C., Rinaldi, M., Decesari, S., Sandrini, S., Costabile, F.,  
675 Gobbi, G.P., Pietrogrande, M.C., Visentin, M., Scotto, F., Fuzzi, S., and Facchini, M.C.: Direct observation of aqueous  
676 secondary organic aerosol from biomass-burning emissions, *PNAS.*, 113, 10013–10018,  
677 <https://doi.org/10.1073/pnas.1602212113>, 2016.
- 678
- 679 Giulianelli, L., Gilardoni, S., Tarozzi, L., Rinaldi, M., Decesari, S., Carbone, C., Facchini, M. C., and Fuzzi, S.: Fog  
680 occurrence and chemical composition in the Po valley over the last twenty years, *Atmos. Environ.*, 98, 394–401,  
681 <https://doi.org/10.1016/j.atmosenv.2014.08.080>, 2014.
- 682
- 683 Gold, M. H., Kutsuki, H., and Morgan, M. A.: Oxidative degradation of lignin by photochemical and chemical radical  
684 generating systems, *Photochem. Photobiol.*, 38, 647–651, <https://doi.org/10.1111/j.1751-1097.1983.tb03595.x>, 1983.
- 685
- 686 Goldstein, S. and Czapski, G.: Kinetics of nitric oxide autoxidation in aqueous solution in the absence and presence of  
687 various reductants. The nature of the oxidizing intermediates, *J. Am. Chem. Soc.*, 117, 12078–12084,  
688 <https://doi.org/10.1021/ja00154a007>, 1995a.
- 689
- 690 Goldstein, S. and Czapski, G.: The reaction of <sup>•</sup>NO with O<sub>2</sub><sup>•-</sup> and <sup>•</sup>HO<sub>2</sub>: a pulse radiolysis study, *Free Radical Biol. Med.*, 19,  
691 505–510, [https://doi.org/10.1016/0891-5849\(95\)00034-U](https://doi.org/10.1016/0891-5849(95)00034-U), 1995b.





- 692 Goldstein, S., Czapski, G., Lind, J., and Merényi, G.: Mechanism of decomposition of peroxyxynitric Ion ( $O_2NOO^-$ ): Evidence  
693 for the formation of  $O_2^*$  and  $^*NO_2$  radicals, *Inorg. Chem.*, 37, 3943–3947, <https://doi.org/10.1021/ic9800511>, 1998.  
694
- 695 Goldstein, S., Lind, J., and Merényi, G.: Chemistry of peroxyxynitrites as compared to peroxyxynitrates, *Chem. Rev.*, 10, 2457–  
696 2470, <https://doi.org/10.1021/cr0307087>, 2005.  
697
- 698 Grosjean, D.: Reactions of o-cresol and nitrocresol with nitrogen oxides ( $NO_x$ ) in sunlight and with ozone–nitrogen dioxide  
699 mixtures in the dark, *Environ. Sci. Technol.*, 19, 968–974, <https://doi.org/10.1021/es00140a014>, 1985.  
700
- 701 Herrmann, H.: On the photolysis of simple anions and neutral molecules as sources of  $O^-/OH$ ,  $SO_x^-$  and Cl in aqueous  
702 solution, *Phys. Chem. Chem. Phys.*, 9, 3935–3964, <https://doi.org/10.1039/B618565G>, 2007.  
703
- 704 Herrmann, H., Hoffmann, D., Schaefer, T., Brüner, P., and Tilgner, A.: Tropospheric aqueous-phase free-radical chemistry:  
705 Radical sources, spectra, reaction kinetics and prediction tools, *Chem Phys Chem.*, 11, 3796–3822,  
706 <https://doi.org/10.1002/cphc.201000533>, 2010.  
707
- 708 Hippelein, M.: Background concentrations of individual and total volatile organic compounds in residential indoor air of  
709 Schleswig-Holstein, Germany, *J. Environ. Monit.*, 6, 745–752, <https://doi.org/10.1039/b401139m>, 2004.  
710
- 711 Hoffer, A., Kiss, G., Blazsó, M., and Gelencsér, A.: Chemical characterization of humic-like substances (HULIS) formed  
712 from a lignin-type precursor in model cloud water, *Geophys. Res. Lett.*, 31, <https://doi.org/10.1029/2003GL018962>, 2004.  
713
- 714 Hoffmann, E.H., Tilgner, A., Wolke, R., Böge, O., Walter, A., and Herrmann, H.: Oxidation of substituted aromatic  
715 hydrocarbons in the tropospheric aqueous phase: kinetic mechanism development and modelling, *Phys. Chem. Chem. Phys.*,  
716 20, 10960–10977, <https://doi.org/10.1039/C7CP08576A>, 2018.  
717
- 718 Holčapek, M., Jirásko, R., and Lída, M.: Basic rules for the interpretation of atmospheric pressure ionization mass spectra of  
719 small molecules, *J. Chromatogr. A*, 1217, 3908–3921, <https://doi.org/10.1016/j.chroma.2010.02.049>, 2010.  
720
- 721 Huang, D. D., Zhang, Q., Cheung, H. H. Y., Yu, L., Zhou, S., Anastasio, C., Smith, J. D., and Chan, C. K.: Formation and  
722 evolution of aqSOA from aqueous-phase reactions of phenolic carbonyls: comparison between ammonium sulfate and  
723 ammonium nitrate solutions, *Environ. Sci. Technol.*, 52, 9215–9224, <https://doi.org/10.1021/acs.est.8b03441>, 2018.  
724
- 725 Huang, J. P. and Mabury, S. A.: The role of carbonate radical in limiting the persistence of sulfur-containing chemicals in  
726 sunlit natural waters, *Chemosphere*, 41, 1775–1782, [https://doi.org/10.1016/S0045-6535\(00\)00042-4](https://doi.org/10.1016/S0045-6535(00)00042-4), 2000.  
727
- 728 Huang, R.-J., Zhang, Y., Bozzetti, C., Ho, K.-F., Cao, J.-J., Han, Y., Daellenbach, K. R., Slowik, J. G., Platt, S. M.,  
729 Canonaco, F., Zotter, P., Wolf, R., Pieber, S. M., Bruns, E. A., Crippa, M., Ciarelli, G., Piazzalunga, A., Schwikowski, M.,  
730 Abbazade, G., Schnelle-Kreis, J., Zimmermann, R., An, Z., Szidat, S., Baltensperger, U., El Haddad, I., and Prévôt, A. S.  
731 H.: High secondary aerosol contribution to particulate pollution during haze events in China, *Nature*, 514, 218–222,  
732 <https://doi.org/10.1038/nature13774>, 2014.  
733
- 734 Huang, X. H. H., Ip, H. S. S., and Yu, J. Z.: Secondary organic aerosol formation from ethylene in the urban atmosphere of  
735 Hong Kong: A multiphase chemical modeling study, *J. Geophys. Res.*, 116, D03206, <https://doi.org/10.1029/2010JD014121>,  
736 2011.  
737
- 738 Jacobson, M. Z.: Isolating nitrated and aromatic aerosols and nitrated aromatic gases as sources of ultraviolet light  
739 absorption, *J. Geophys. Res.*, 104, 3527–3542, <https://doi.org/10.1029/1998JD100054>, 1999.



- 740 Jiang, W., Misovich, M. V., Hettiyadura, A. P. S., Laskin, A., McFall, A. S., Anastasio, C., and Zhang, Q.: Photosensitized  
741 reactions of a phenolic carbonyl from wood combustion in the aqueous phase—chemical evolution and light absorption  
742 properties of aqSOA, *Environ. Sci. Technol.*, 55, 5199–5211, <https://doi.org/10.1021/acs.est.0c07581>, 2021.  
743
- 744 Jimenez, J. L., Canagaratna, M. R., Donahue, N. M., Prevot, A.S.H., Zhang, Q., Kroll, J. H., DeCarlo, P. F., Allan, J. D.,  
745 Coe, H., Ng, N. L., Aiken, A.C., Docherty, K.S., Ulbrich, I. M., Grieshop, A. P., Robinson, A. L., Duplissy, J., Smith, J. D.,  
746 Wilson, K. R., Lanz, V.A., Hueglin, C., Sun, Y. L., Tian, J., Laaksonen, A., Raatikainen, T., Rautiainen, J., Vaattovaara, P.,  
747 Ehn, M., Kulmala, M., Tomlinson, J. M., Collins, D. R., Cubison, M. J., Dunlea, E. J., Huffman, J. A., Onasch, T. B.,  
748 Alfarra, M. R., Williams, P. I., Bower, K., Kondo, Y., Schneider, J., Drewnick, F., Borrmann, S., Weimer, S., Demerjian, K.,  
749 Salcedo, D., Cottrell, L., Griffin, R., Takami, A., Miyoshi, T., Hatakeyama, S., Shimono, A., Sun, J. Y., Zhang, Y. M.,  
750 Dzepina, K., Kimmel, J. R., Sueper, D., Jayne, J. T., Herndon, S. C., Trimborn, A. M., Williams, L. R., Wood, E. C.,  
751 Middlebrook, A. M., Kolb, C. E., Baltensperger, U., and Worsnop, D. R.: Evolution of organic aerosols in the atmosphere,  
752 *Science*, 326, 1525–1529, <https://doi.org/10.1126/science.1180353>, 2009.  
753
- 754 Jung, H., Chadha, T. S., Kim, D., Biswas, P., and Jun, Y.-S.: Photochemically assisted fast abiotic oxidation of manganese  
755 and formation of  $\delta$ -MnO<sub>2</sub> nanosheets in nitrate solution, *Chem. Commun.*, 53, 4445–4448,  
756 <https://doi.org/10.1039/C7CC00754J>, 2017.  
757
- 758 Kahnt, A., Behrouzi, S., Vermeylen, R., Shalamzari, M. S., Vercauteren, J., Roekens, E., Claeys, M., and Maenhaut, W.:  
759 One-year study of nitro-organic compounds and their relation to wood burning in PM<sub>10</sub> aerosol from a rural site in Belgium,  
760 *Atmos. Environ.*, 81, 561–568, <https://doi.org/10.1016/j.atmosenv.2013.09.041>, 2013.  
761
- 762 Kanakidou, M., Seinfeld, J. H., Pandis, S. N., Barnes, I., Dentener, F. J., Facchini, M. C., Van Dingenen, R., Ervens, B.,  
763 Nenes, A., Nielsen, C. J., Swietlicki, E., Putaud, J. P., Balkanski, Y., Fuzzi, S., Horth, J., Moortgat, G. K., Winterhalter, R.,  
764 Myhre, C. E. L., Tsigaridis, K., Vignati, E., Stephanou, E. G., and Wilson, J.: Organic aerosol and global climate modelling:  
765 a review, *Atmos. Chem. Phys.*, 5, 1053–1123, <https://doi.org/10.5194/acp-5-1053-2005>, 2005.  
766
- 767 Kaur, R. and Anastasio, C.: First measurements of organic triplet excited states in atmospheric waters, *Environ. Sci.*  
768 *Technol.*, 52, 5218–5226, <https://doi.org/10.1021/acs.est.7b06699>, 2018.  
769
- 770 Kaur, R., Labins, J. R., Helbock, S. S., Jiang, W., Bein, K. J., Zhang, Q., and Anastasio, C.: Photooxidants from brown  
771 carbon and other chromophores in illuminated particle extracts, *Atmos. Chem. Phys.*, 19, 6579–6594,  
772 <https://doi.org/10.5194/acp-19-6579-2019>, 2019.  
773
- 774 Kebarle, P. A.: A brief overview of the mechanisms involved in electrospray mass spectrometry, *J. Mass Spectrom.*, 35,  
775 804–817, <https://doi.org/10.1002/9783527628728.ch1>, 2000.  
776
- 777 Kim, D.-h., Lee, J., Ryu, J., Kim, K., and Choi, W.: Arsenite oxidation initiated by the UV photolysis of nitrite and nitrate,  
778 *Environ. Sci. Technol.*, 48, 4030–4037, <https://doi.org/10.1021/es500001q>, 2014.  
779
- 780 Kitanovski, Z., Čusak, A., Grgić, I., and Claeys, M.: Chemical characterization of the main products formed through  
781 aqueous-phase photonitration of guaiaicol, *Atmos. Meas. Tech.*, 7, 2457–2470, <https://doi.org/10.5194/amt-7-2457-2014>,  
782 2014.  
783
- 784 Klodt, A.L., Romonosky, D.E., Lin, P., Laskin, J., Laskin, A., and Nizkorodov, S.A.: Aqueous photochemistry of secondary  
785 organic aerosol of  $\alpha$ -pinene and  $\alpha$ -humulene in the presence of hydrogen peroxide or inorganic salts, *ACS Earth Space*  
786 *Chem.*, 3, 12, 2736–2746, <https://doi.org/10.1021/acsearthspacechem.9b00222>, 2019.  
787
- 788 Kourtchev, I., Fuller, S. J., Giorio, C., Healy, R. M., Wilson, E., O'Connor, I., Wenger, J. C., McLeod, M., Aalto, J.,  
789 Ruuskanen, T. M., Maenhaut, W., Jones, R., Venables, D. S., Sodeau, J. R., Kulmala, M., and Kalberer, M.: Molecular



- 790 composition of biogenic secondary organic aerosols using ultrahigh-resolution mass spectrometry: comparing laboratory and  
791 field studies, *Atmos. Chem. Phys.*, 14, 2155–2167, <https://doi.org/10.5194/acp-14-2155-2014>, 2014.  
792
- 793 Kroflič, A., Grilc, M., and Grgić, I.: Unraveling pathways of guaiacol nitration in atmospheric waters: nitrite, a source of  
794 reactive nitronium ion in the atmosphere, *Environ. Sci. Technol.*, 49, 9150–9158, <https://doi.org/10.1021/acs.est.5b01811>,  
795 2015.  
796
- 797 Kroflič, A., Anders, J., Drventić, I., Mettke, P., Böge, O., Mutzel, A., Kleffmann, J., and Herrmann, H.: Guaiacol nitration in  
798 a simulated atmospheric aerosol with an emphasis on atmospheric nitrophenol formation mechanisms, *ACS Earth Space*  
799 *Chem.*, <https://doi.org/10.1021/acsearthspacechem.1c00014>, 2021.  
800
- 801 Kroll, J. H., Donahue, N. M., Jimenez, J. L., Kessler, S. H., Canagaratna, M. R., Wilson, K. R., Altieri, K. E., Mazzoleni, L.  
802 R., Wozniak, A. S., Bluhm, H., Mysak, E. R., Smith, J. D., Kolb, C. E., and Worsnop, D. R.: Carbon oxidation state as a  
803 metric for describing the chemistry of atmospheric organic aerosol, *Nat. Chem.*, 3, 133–139,  
804 <https://doi.org/10.1038/nchem.948>, 2011.  
805
- 806 Lammel, G., Perner, D., and Warneck, P.: Decomposition of pernitric acid in aqueous solution, *J. Phys. Chem.*, 94,  
807 6141–6144, <https://doi.org/10.1021/j100378a091>, 1990.  
808
- 809 Laskin, A., Laskin, J., and Nizkorodov, S.A.: Chemistry of atmospheric brown carbon, *Chem. Rev.*, 115, 4335–4382,  
810 <https://doi.org/10.1021/cr5006167>, 2015.  
811
- 812 LeClair, J. P., Collett, J. L., and Mazzoleni, L. R.: Fragmentation analysis of water-soluble atmospheric organic matter using  
813 ultrahigh-resolution FT-ICR mass spectrometry, *Environ. Sci. Technol.*, 46, 4312–4322, <https://doi.org/10.1021/es203509b>,  
814 2012.  
815
- 816 Lee, A. K. Y., Herckes, P., Leaitch, W. R., Macdonald, A. M., and Abbatt, J. P. D.: Aqueous OH oxidation of ambient  
817 organic aerosol and cloud water organics: Formation of highly oxidized products, *Geophys. Res. Lett.*, 38, L11805,  
818 <https://doi.org/10.1029/2011GL047439>, 2011.  
819
- 820 Lee, A. K. Y., Zhao, R., Li, R., Liggio, J., Li, S.-M., and Abbatt, J. P. D.: Formation of light absorbing organo-nitrogen  
821 species from evaporation of droplets containing glyoxal and ammonium sulfate, *Environ. Sci. Technol.*, 47, 12819–12826,  
822 <https://doi.org/10.1021/es402687w>, 2013.  
823
- 824 Lee, P. C. C. and Rodgers, M. A. J.: Laser flash photokinetic studies of Rose Bengal sensitized photodynamic interactions of  
825 nucleotides and DNA, *Photochem. Photobiol.*, 45, 79–86, <https://doi.org/10.1111/j.1751-1097.1987.tb08407.x>, 1987.  
826
- 827 Lewis, A. C., Hopkins, J. R., Carslaw, D. C., Hamilton, J. F., Nelson, B. S., Stewart, G., Dernie, J., Passant, N., and Murrells,  
828 T.: An increasing role for solvent emissions and implications for future measurements of volatile organic compounds, *Philos.*  
829 *Trans. R. Soc.*, 378, <https://doi.org/10.1098/rsta.2019.0328>, 2020.  
830
- 831 Li, F., Tang, S., Tsona, N. T., and Du, L.: Kinetics and mechanism of OH-induced  $\alpha$ -terpineol oxidation in the atmospheric  
832 aqueous phase, *Atmos. Environ.*, 237, 117650, <https://doi.org/10.1016/j.atmosenv.2020.117650>, 2020.  
833
- 834 Li, P., Li, X., Yang, C., Wang, X., Chen, J., and Collett, J. L. Jr.: Fog water chemistry in Shanghai, *Atmos. Environ.*, 45,  
835 4034–4041, <https://doi.org/10.1016/j.atmosenv.2011.04.036>, 2011.  
836
- 837 Li, Y. J., Huang, D. D., Cheung, H. Y., Lee, A. K. Y., and Chan, C. K.: Aqueous-phase photochemical oxidation and direct  
838 photolysis of vanillin - a model compound of methoxy phenols from biomass burning, *Atmos. Chem. Phys.*, 14, 2871–2885,  
839 <https://doi.org/10.5194/acp-14-2871-2014>, 2014.



- 840 Liang, Z., Zhang, R., Gen, M., Chu, Y., and Chan, C. K.: Nitrate photolysis in mixed sucrose–nitrate–sulfate particles at  
841 different relative humidities, *J. Phys. Chem. A*, 125, 3739–3747, <https://doi.org/10.1021/acs.jpca.1c00669>, 2021.
- 842
- 843 Liigand, P., Kaupmees, K., Haav, K., Liigand, J., Leito, I., Girod, M., Antoine, R., and Kruve, A.: Think negative: finding  
844 the best electrospray ionization/MS mode for your analyte, *Anal. Chem.*, 89, 5665–5668,  
845 <https://doi.org/10.1021/acs.analchem.7>, 2017.
- 846
- 847 Lim, Y. B., Tan, Y., Perri, M. J., Seitzinger, S. P., and Turpin, B. J.: Aqueous chemistry and its role in secondary organic  
848 aerosol (SOA) formation, *Atmos. Chem. Phys.*, 10, 10521–10539, <https://doi.org/10.5194/acp-10-10521-2010>, 2010.
- 849
- 850 Lin, P., Yu, J. Z., Engling, G., and Kalberer, M.: Organosulfates in humic-like substance fraction isolated from aerosols at  
851 seven locations in East Asia: a study by ultra-high-resolution mass spectrometry, *Environ. Sci. Technol.*, 46, 13118–13127,  
852 <https://doi.org/10.1021/es303570v>, 2012.
- 853
- 854 Lin, P., Fleming, L. T., Nizkorodov, S. A., Laskin, J., and Laskin, A.: Comprehensive molecular characterization of  
855 atmospheric brown carbon by high resolution mass spectrometry with electrospray and atmospheric pressure photoionization,  
856 *Anal. Chem.*, 90, 12493–12502, <https://doi.org/10.1021/acs.analchem.8b02177>, 2018.
- 857
- 858 Liu, C., Liu, J., Liu, Y., Chen, T., and He, H.: Secondary organic aerosol formation from the OH-initiated oxidation of  
859 guaiacol under different experimental conditions, *Atmos. Environ.*, 207, 30–37,  
860 <https://doi.org/10.1016/j.atmosenv.2019.03.021>, 2019.
- 861
- 862 Lobodin, V. V., Marshall, A. G., and Hsu, C. S.: Compositional space boundaries for organic compounds, *Anal. Chem.*, 84,  
863 3410–3416, <https://doi.org/10.1021/ac300244f>, 2012.
- 864
- 865 Loisel, G., Mekic, M., Liu, S., Song, W., Jiang, B., Wang, Y., Deng, H., and Gligorovski, S.: Ionic strength effect on the  
866 formation of organonitrate compounds through photochemical degradation of vanillin in liquid water of aerosols, *Atmos.*  
867 *Environ.*, 246, 118140, <https://doi.org/10.1016/j.atmosenv.2020.118140>, 2021.
- 868
- 869 Ma, L., Guzman, C., Niedek, C., Tran, T., Zhang, Q., and Anastasio, C.: Kinetics and mass yields of aqueous secondary  
870 organic aerosol from highly substituted phenols reacting with a triplet excited state, *Environ. Sci. Technol.*, 55, 5772–5781,  
871 <https://doi.org/10.1021/acs.est.1c00575>, 2021.
- 872
- 873 Mabato, B. R. G., Gen, M., Chu, Y., and Chan, C. K.: Reactive uptake of glyoxal by methylammonium-containing salts as a  
874 function of relative humidity, *ACS Earth Space Chem.*, 3, 150–157, <https://doi.org/10.1021/acsearthspacechem.8b00154>,  
875 2019.
- 876
- 877 Machado, F. and Boule, P.: Photonitration and photonitrosation of phenolic derivatives induced in aqueous solution by  
878 excitation of nitrite and nitrate ions, *J. Photochem. Photobiol. A: Chem.*, 86, 73–80, [https://doi.org/10.1016/1010-6030\(94\)03946-R](https://doi.org/10.1016/1010-6030(94)03946-R), 1995.
- 880
- 881 Mack, J. and Bolton, J.R.: Photochemistry of nitrite and nitrate in aqueous solution: a review, *J. Photochem. Photobiol.*  
882 *Chem.*, 128, 1–13, [https://doi.org/10.1016/S1010-6030\(99\)00155-0](https://doi.org/10.1016/S1010-6030(99)00155-0), 1999.
- 883
- 884 Mazzoleni, L. R., Saranjampour, P., Dalbec, M. M., Samburova, V., Hallar, A. G., Zielinska, B., Lowenthal, D. H., and  
885 Kohl, S.: Identification of water-soluble organic carbon in non-urban aerosols using ultrahigh-resolution FT-ICR mass  
886 spectrometry: organic anions, *Environ. Chem.*, 9, 285–297, <https://doi.org/10.1071/EN11167>, 2012.
- 887
- 888 McFall, A. S., Johnson, A. W., and Anastasio, C.: Air–water partitioning of biomass-burning phenols and the effects of  
889 temperature and salinity, *Environ. Sci. Technol.*, 54, 3823–3830, <https://doi.org/10.1021/acs.est.9b06443>, 2020.



- 890 Minero, C., Bono, F., Rubertelli, F., Pavino, D., Maurino, V., Pelizzetti, E., and Vione, D.: On the effect of pH in aromatic  
891 photonitration upon nitrate photolysis, *Chemosphere*, 66, 650–656, <https://doi.org/10.1016/j.chemosphere.2006.07.082>, 2007.  
892
- 893 Mohr, C., Lopez-Hilfiker, F. D., Zotter, P., Prévôt, A. S. H., Xu, L., Ng, N. L., Herndon, S. C., Williams, L. R., Franklin, J.  
894 P., Zahniser, M. S., Worsnop, D. R., Knighton, W. B., Aiken, A. C., Gorkowski, K. J., Dubey, M. K., Allan, J. D., and  
895 Thornton, J. A.: Contribution of nitrated phenols to wood burning brown carbon light absorption in Detling, United  
896 Kingdom during winter time, *Environ. Sci. Technol.*, 47, 6316–6324, <https://doi.org/10.1021/es400683v>, 2013.  
897
- 898 Munger, J. W., Jacob, D. J., Waldman, J. M., and Hoffmann, M. R.: Fogwater chemistry in an urban atmosphere, *J.*  
899 *Geophys. Res. Oceans*, 88, 5109–5121, <https://doi.org/10.1029/JC088iC09p05109>, 1983.  
900
- 901 Neta, P., Huie, R. E., and Ross, A.: Rate constants for reactions of inorganic radicals in aqueous solution, *J. Phys. Chem.*  
902 *Ref. Data*, 17, 1027–1284, <https://doi.org/10.1063/1.555808>, 1988.  
903
- 904 Nolte, C. G., Schauer, J. J., Cass, G. R., and Simoneit, B. R. T.: Highly polar organic compounds present in wood smoke and  
905 in the ambient atmosphere, *Environ. Sci. Technol.*, 35, <https://doi.org/10.1021/es001420r>, 1912–1919, 2001.  
906
- 907 Nozière, B., Dziedzic, P., and Córdova, A.: Products and kinetics of the liquid-phase reaction of glyoxal catalyzed by  
908 ammonium ions ( $\text{NH}_4^+$ ), *J. Phys. Chem. A*, 113, 231–237, <https://doi.org/10.1021/jp8078293>, 2009.  
909
- 910 Olofsson, M., Ek-Olausson, B., Ljungström, E., and Langer, S.: Flux of organic compounds from grass measured by relaxed  
911 eddy accumulation technique, *J. Environ. Monit.*, 5, 963–970, <https://doi.org/10.1039/B303329E>, 2003.  
912
- 913 Onori, G. and Santucci, A.: Dynamical and structural properties of water/alcohol mixtures, *J. Mol. Liq.*, 69, 161–181,  
914 [https://doi.org/10.1016/S0167-7322\(96\)90012-4](https://doi.org/10.1016/S0167-7322(96)90012-4), 1996.  
915
- 916 Pang, H., Zhang, Q., Lu, X. H., Li, K., Chen, H., Chen, J., Yang, X., Ma, Y., Ma, J., and Huang, C.: Nitrite-mediated  
917 photooxidation of vanillin in the atmospheric aqueous phase, *Environ. Sci. Technol.*, 53, 14253–14263,  
918 <https://doi.org/10.1021/acs.est.9b03649>, 2019a.  
919
- 920 Pang, H., Zhang, Q., Wang, H., Cai, D., Ma, Y., Li, L., Li, K., Lu, X., Chen, H., Yang, X., and Chen, J.: Photochemical  
921 aging of guaiacol by Fe(III)-oxalate complexes in atmospheric aqueous phase, *Environ. Sci. Technol.*, 53, 127–136,  
922 <https://doi.org/10.1021/acs.est.8b04507>, 2019b.  
923
- 924 Powelson, M. H., Espelien, B. M., Hawkins, L. N., Galloway, M. M., and De Haan, D. O.: Brown carbon formation by  
925 aqueous-phase carbonyl compound reactions with amines and ammonium sulfate, *Environ. Sci. Technol.*, 48, 985–993,  
926 <https://doi.org/10.1021/es4038325>, 2014.  
927
- 928 Pöschl, U.: Atmospheric aerosols: composition, transformation, climate, and health effects, *Angew. Chem. Int.*, 44, 7520–  
929 7540, <https://doi.org/10.1002/anie.200501122>, 2005.  
930
- 931 Priya, A. M. and Lakshmipathi, S.: DFT study on abstraction reaction mechanism of oh radical with 2-methoxyphenol, *J.*  
932 *Phys. Org. Chem.*, 30, <https://doi.org/10.1002/poc.3713>, 2017.  
933
- 934 Pye, H., Nenes, A., Alexander, B., Ault, A. P., Barth, M. C., Clegg, S. L., Collett, J. L. Jr., Fahey, K. M., Hennigan, C. J.,  
935 Herrmann, H., Kanakidou, M., Kelly, J. T., Ku, I. T., McNeill, V. F., Riemer, N., Schaefer, T., Shi, G., Tilgner, A., Walker,  
936 J. T., Wang, T., Weber, R., Xing, J., Zaveri, R. A., and Zuend, A.: The acidity of atmospheric particles and clouds, *Atmos.*  
937 *Chem. Phys.*, 20, 4809–4888, <https://doi.org/10.5194/acp-20-4809-2020>, 2020.





- 938 Qi, L., Chen, M., Stefenelli, G., Pospisilova, V., Tong, Y., Bertrand, A., Hueglin, C., Ge, X., Baltensperger, U., Prévôt, A. S.  
939 H., and Slowik, J.G.: Organic aerosol source apportionment in Zurich using an extractive electrospray ionization time-of-  
940 flight mass spectrometer (EESI-TOF-MS) — Part 2: Biomass burning influences in winter, *Atmos. Chem. Phys.*, 19, 8037–  
941 8062, <https://doi.org/10.5194/acp-19-8037-2019>, 2019.
- 942
- 943 Rizzo, L.V., Artaxo, P., Karl, T., Guenther, A.B., and Greenberg, J.: Aerosol properties, in-canopy gradients, turbulent  
944 fluxes and VOC concentrations at a pristine forest site in Amazonia, *Atmos. Environ.*, 44, 503-511,  
945 <https://doi.org/10.1016/j.atmosenv.2009.11.002>, 2010.
- 946
- 947 Rogge, W. F., Hildemann, L. M., Mazurek, M. A., Cass, G. R., and Simoneit, B. R. T.: Sources of fine organic aerosol. 9.  
948 Pine, oak, and synthetic log combustion in residential fireplaces, *Environ. Sci. Technol.*, 32, 13–22,  
949 <https://doi.org/10.1021/es960930b>, 1998.
- 950
- 951 Scharko, N. K., Berke, A. E., and Raff, J. D.: Release of nitrous acid and nitrogen dioxide from nitrate photolysis in acidic  
952 aqueous solutions, *Environ. Sci. Technol.*, 48, 20, 11991–1200, <https://doi.org/10.1021/es503088x>, 2014.
- 953
- 954 Schauer, J. J., Kleeman, M. J., Cass, G. R., and Simoneit, B. R. T.: Measurement of emissions from air pollution sources. 3.  
955 C<sub>1</sub>–C<sub>29</sub> organic compounds from fireplace combustion of wood, *Environ. Sci. Technol.*, 35, 1716–1728,  
956 <https://doi.org/10.1021/es001331e>, 2001.
- 957
- 958 Sedehi, N., Takano, H., Blasic, V. A., Sullivan, K. A., and De Haan, D. O.: Temperature- and pH-dependent aqueous-phase  
959 kinetics of the reactions of glyoxal and methylglyoxal with atmospheric amines and ammonium sulfate, *Atmos. Environ.*, 77,  
960 656–663, <https://doi.org/10.1016/j.atmosenv.2013.05.070>, 2013.
- 961
- 962 Shapiro, E. L., Szprengiel, J., Sareen, N., Jen, C. N., Giordano, M. R., and McNeill, V. F.: Light-absorbing secondary  
963 organic material formed by glyoxal in aqueous aerosol mimics, *Atmos. Chem. Phys.*, 9, 2289–2300,  
964 <https://doi.org/10.5194/acp-9-2289-2009>, 2009.
- 965
- 966 Siegmann, K. and Sattler, K. D.: Formation mechanism for polycyclic aromatic hydrocarbons in methane flames, *J. Chem.*  
967 *Phys.*, 112, 698–709, <https://doi.org/10.1063/1.480648>, 2000.
- 968
- 969 Slikboer, S., Grandy, L., Blair, S. L., Nizkorodov, S. A., Smith, R. W., and Al-Abadleh, H. A.: Formation of light absorbing  
970 soluble secondary organics and insoluble polymeric particles from the dark reaction of catechol and guaiacol with Fe(III),  
971 *Environ. Sci. Technol.*, 49, 7793–7801, <https://doi.org/10.1021/acs.est.5b01032>, 2015.
- 972
- 973 Smith, J. D., Sio, V., Yu, L., Zhang, Q., and Anastasio, C.: Secondary organic aerosol production from aqueous reactions of  
974 atmospheric phenols with an organic triplet excited state, *Environ. Sci. Technol.*, 48, 1049–1057,  
975 <https://doi.org/10.1021/es4045715>, 2014.
- 976
- 977 Smith, J. D., Kinney, H., and Anastasio, C.: Aqueous benzene-diols react with an organic triplet excited state and hydroxyl  
978 radical to form secondary organic aerosol, *Phys. Chem. Chem. Phys.*, 17, 10227–10237,  
979 <https://doi.org/10.1039/C4CP06095D>, 2015.
- 980
- 981 Smith, J. D., Kinney, H., and Anastasio, C.: Phenolic carbonyls undergo rapid aqueous photodegradation to form low-  
982 volatility, light-absorbing products, *Atmos. Environ.*, 126, 36–44, <https://doi.org/10.1016/j.atmosenv.2015.11.035>, 2016.
- 983
- 984 Straub, D. J.: Radiation fog chemical composition and its temporal trend over an eight year period, *Atmos. Environ.*, 148,  
985 49–61, <https://doi.org/10.1016/j.atmosenv.2016.10.031>, 2017.





- 986 Straub, D. J., Hutchings, J. W., and Herckes, P.: Measurements of fog composition at a rural site, *Atmos. Environ.*, **47**, 195–  
987 205., <https://doi.org/10.1016/j.atmosenv.2011.11.014>, 2012.
- 988
- 989 Sturzbecher-Höhne, M., Nauser, T., Kissner, R., and Koppenol, W. H.: Photon-initiated homolysis of peroxyxynitrous acid,  
990 *Inorg. Chem.*, **48**, 7307–7312, <https://doi.org/10.1021/ic900614e>, 2009.
- 991
- 992 Sun, Y., Xu, F., Li, X., Zhang, Q., and Gu, Y.: Mechanisms and kinetic studies of OH-initiated atmospheric oxidation of  
993 methoxyphenols in the presence of O<sub>2</sub> and NO<sub>x</sub>, *Phys. Chem. Chem. Phys.*, **21**, 21856–21866,  
994 <https://doi.org/10.1039/C9CP03246K>, 2019.
- 995
- 996 Sun, Y. L., Zhang, Q., Anastasio, C., and Sun, J.: Insights into secondary organic aerosol formed via aqueous-phase  
997 reactions of phenolic compounds based on high resolution mass spectrometry, *Atmos. Chem. Phys.*, **10**, 4809–4822,  
998 <https://doi.org/10.5194/acp-10-4809-2010>, 2010.
- 999
- 1000 Teich, M., van Pinxteren, D., Wang, M., Kecorius, S., Wang, Z., Müller, T., Močnik, G., and Herrmann, H.: Contributions of  
1001 nitrated aromatic compounds to the light absorption of water-soluble and particulate brown carbon in different atmospheric  
1002 environments in Germany and China, *Atmos. Chem. Phys.*, **17**, 1653–1672, <https://doi.org/10.5194/acp-17-1653-2017>, 2017.
- 1003
- 1004 Tinel, L., George, C., Brüggemann, M., Hayeck, N., and Donaldson, D. J.: Interfacial photochemistry: physical chemistry of  
1005 gas-liquid interfaces, in: *Developments in Physical & Theoretical Chemistry*, edited by: Faust, J. A. and House, J. E.,  
1006 Elsevier, 435–457, <https://doi.org/10.1016/B978-0-12-813641-6.00014-5>, 2018.
- 1007
- 1008 Vione, D., Maurino, V., Minero, C., and Pelizzetti, E.: Phenol photolysis upon UV irradiation of nitrite in aqueous  
1009 solution I: effects of oxygen and 2-propanol, *Chemosphere*, **45**, 893–902, [https://doi.org/10.1016/S0045-6535\(01\)00035-2](https://doi.org/10.1016/S0045-6535(01)00035-2),  
1010 2001.
- 1011
- 1012 Vione, D., Maurino, V., Minero, C., and Pelizzetti, E.: Reactions induced in natural waters by irradiation of nitrate and nitrite  
1013 ions, in: *The Handbook of Environmental Chemistry Vol. 2M - Environmental Photochemistry Part II*, Springer, Berlin,  
1014 Heidelberg, Germany, 221–253, <https://doi.org/10.1007/b138185>, 2005.
- 1015
- 1016 Vione, D., Maurino, V., Minero, C., Pelizzetti, E., Harrison, M. A. J., Olariu, R., and Arsene, C.: Photochemical reactions in  
1017 the tropospheric aqueous phase and on particulate matter, *Chem. Soc. Rev.*, **35**, 441–453, <https://doi.org/10.1039/B510796M>,  
1018 2006.
- 1019
- 1020 Vione, D., Khanra, S., Cucu-Man, S., Maddigapu, P. R., Das, R., Arsene, C., Olariu, R.-I., Maurino, V., and Minero, C.:  
1021 Inhibition vs. enhancement of the nitrate-induced phototransformation of organic substrates by the 'OH scavengers  
1022 bicarbonate and carbonate, *Water Res.*, **43**, 4718–4728, <https://doi.org/10.1016/j.watres.2009.07.032>, 2009.
- 1023
- 1024 Vione, D., Albinet, A., Barsotti, F., Mekic, M., Jiang, B., Minero, C., Brigante, M., and Gligorovski, S.: Formation of  
1025 substances with humic-like fluorescence properties, upon photoinduced oligomerization of typical phenolic compounds  
1026 emitted by biomass burning, *Atmos. Environ.*, **206**, 197–207, <https://doi.org/10.1016/j.atmosenv.2019.03.005>, 2019.
- 1027
- 1028 Volkamer, R., Ziemann, P. J., Molina, and M. J.: Secondary organic aerosol formation from acetylene (C<sub>2</sub>H<sub>2</sub>): seed effect on  
1029 SOA yields due to organic photochemistry in the aerosol aqueous phase, *Atmos. Chem. Phys.*, **9**, 1907–1928,  
1030 <https://doi.org/10.5194/acp-9-1907-2009>, 2009.
- 1031
- 1032 Wang, X., Dalton, E. Z., Payne, Z. C., Perrier, S., Riva, M., Raff, J. D., and George, C.: Superoxide and nitrous acid  
1033 production from nitrate photolysis is enhanced by dissolved aliphatic organic matter, *Environ. Sci. Technol. Lett.*, **8**, 53–58,  
1034 <https://doi.org/10.1021/acs.estlett.0c00806>, 2021.



- 1035 Warneck, P. and Wurzinger, C.: Product quantum yields for the 305-nm photodecomposition of nitrate in aqueous solution, *J.*  
1036 *Phys. Chem.*, 92, 6278–6283, <https://doi.org/10.1021/j100333a022>, 1988.  
1037
- 1038 Williams, D. H. and Fleming, I.: Spectroscopic methods in organic chemistry, 6th Ed., McGraw-Hill Education, London,  
1039 2008.  
1040
- 1041 Wojnárovits, L., Tóth, T., and Takács, E.: Rate constants of carbonate radical anion reactions with molecules of  
1042 environmental interest in aqueous solution: a review, *Sci. Total Environ.*, 717, 137219,  
1043 <https://doi.org/10.1016/j.scitotenv.2020.137219>, 2020.  
1044
- 1045 Xie, Q., Su, S., Chen, S., Xu, Y., Cao, D., Chen, J., Ren, L., Yue, S., Zhao, W., Sun, Y., Wang, Z., Tong, H., Su, H., Cheng,  
1046 Y., Kawamura, K., Jiang, G., Liu, C-Q., and Fu, P.: Molecular characterization of firework-related urban aerosols using  
1047 Fourier transform ion cyclotron resonance mass spectrometry, *Atmos. Chem. Phys.*, 20, 6803–6820, [10.5194/acp-2019-  
1048 1180](https://doi.org/10.5194/acp-2019-1180), <https://doi.org/10.5194/acp-20-6803-2020>, 2020.  
1049
- 1050 Yang, J., Au, W. C., Law, H., Lam, C. H., and Nah, T.: Formation and evolution of brown carbon during aqueous-phase  
1051 nitrate-mediated photooxidation of guaiacol and 5-nitroguaiacol, *Atmos. Environ.*, 254, 118401,  
1052 <https://doi.org/10.1016/j.atmosenv.2020.118140>, 2021.  
1053
- 1054 Yaremenko, I. A., Vil', V. A., Demchuk, D. V., and Terent'ev, A. O.: Rearrangements of organic peroxides and related  
1055 processes, *Beilstein J. Org. Chem.*, 12., 1647–1748, <https://doi.org/10.3762/bjoc.12.162>, 2016.  
1056
- 1057 Yaws, C. L.: Handbook of vapor pressure: Volume 3: Organic compounds C<sub>8</sub> to C<sub>28</sub>, Gulf Professional Publishing, USA,  
1058 1994.  
1059
- 1060 Ye, Z., Qu, Z., Ma, S., Luo, S., Chen, Y., Chen, H., Chen, Y., Zhao, Z., Chen, M., and Ge, X.: A comprehensive  
1061 investigation of aqueous-phase photochemical oxidation of 4-ethylphenol, *Sci. Total Environ.*, 685, 976–985,  
1062 <https://doi.org/10.1016/j.scitotenv.2019.06.276>, 2019.  
1063
- 1064 Yu, G., Bayer, A. R., Galloway, M. M., Korshavn, K. J., Fry, C. G., and Keutsch, F. N.: Glyoxal in aqueous ammonium  
1065 sulfate solutions: products, kinetics and hydration effects, *Environ. Sci. Technol.*, 45, 6336–6342,  
1066 <https://doi.org/10.1021/es200989n>, 2011.  
1067
- 1068 Yu, L., Smith, J., Laskin, A., Anastasio, C., Laskin, J., and Zhang, Q.: Chemical characterization of SOA formed from  
1069 aqueous-phase reactions of phenols with the triplet excited state of carbonyl and hydroxyl radical, *Atmos. Chem. Phys.*, 14,  
1070 13801–13816, <https://doi.org/10.5194/acp-14-13801-2014>, 2014.  
1071
- 1072 Zhang, Q. and Anastasio, C.: Conversion of fogwater and aerosol organic nitrogen to ammonium, nitrate, and NO<sub>x</sub> during  
1073 exposure to simulated sunlight and ozone, *Environ. Sci. Technol.*, 37, 3522–3530, <https://doi.org/10.1021/es034114x>, 2003.  
1074
- 1075 Zhang, R., Gen, M., Fu, T-M., and Chan, C. K.: Production of formate via oxidation of glyoxal promoted by particulate  
1076 nitrate photolysis, *Environ. Sci. Technol.*, 55, 5711–5720, <https://doi.org/10.1021/acs.est.0c08199>, 2021.  
1077
- 1078 Zhao, R., Lee, A. K. Y., Huang, L., Li, X., Yang, F., and Abbatt, J. P. D.: Photochemical processing of aqueous atmospheric  
1079 brown carbon, *Atmos. Chem. Phys.*, 15, 6087–6100, <https://doi.org/10.5194/acp-15-6087-2015>, 2015.  
1080
- 1081 Zhao, Y., Hallar, A.G., and Mazzoleni, L.R.: Atmospheric organic matter in clouds: exact masses and molecular formula  
1082 identification using ultrahigh-resolution FT-ICR mass spectrometry, *Atmos. Chem. Phys.* 13, 12343–12362,  
1083 <https://doi.org/10.5194/acp-13-12343-2013>, 2013.



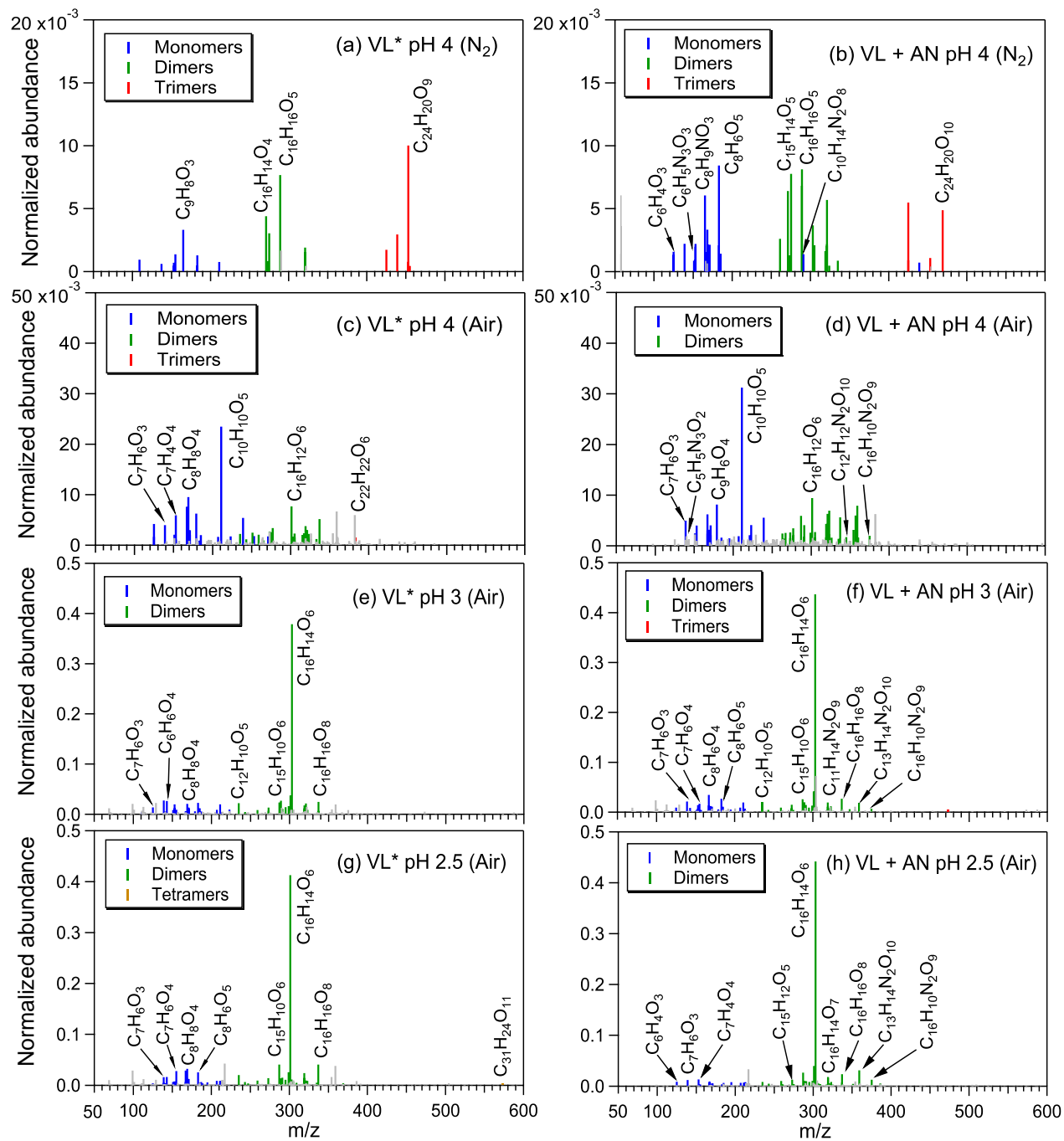
- 1084 Zhou, W., Mekic, M., Liu, J., Loisel, G., Jin, B., Vione, D., and Gligorovski, S.: Ionic strength effects on the photochemical  
1085 degradation of acetosyringone in atmospheric deliquescent aerosol particles, *Atmos. Environ.*, 198, 83–88,  
1086 <https://doi.org/10.1016/j.atmosenv.2018.10.047>, 2019.  
1087
- 1088 Zielinski, T., Bolzacchini, E., Cataldi, M., Ferrero, L., Graßl, S., Hansen, G., Mateos, D., Mazzola, M., Neuber, R., Pakszys,  
1089 P., Posyniak, M., Ritter, C., Severi, M., Sobolewski, P., Traversi, R., and Velasco-Merino, C.: Study of chemical and optical  
1090 properties of biomass burning aerosols during long-range transport events toward the Arctic in summer 2017, *Atmosphere*,  
1091 11, 84, <https://doi.org/10.3390/atmos11010084>, 2020.  
1092
- 1093 Ziemann, P. J. and Atkinson, R.: Kinetics, products, and mechanisms of secondary organic aerosol formation, *Chem. Soc.*  
1094 *Rev.*, 41, 6582–6605, <https://doi.org/10.1039/C2CS35122F>, 2012.



1095 **Table 1.** List of reactions involving reactive species relevant to this study.

No.	Reactions	References
1	$\text{NO}_3^- + h\nu \rightarrow \cdot\text{NO}_2 + \text{O}^-; \phi = 0.01$	Vione et al., 2006; Scharko et al., 2014
2	$\text{O}^- + \text{H}_3\text{O}^+ \leftrightarrow \cdot\text{OH} + \text{H}_2\text{O}$	
3	$\text{NO}_3^- + h\nu \rightarrow \text{NO}_2^- + \text{O}(^3\text{P}); \phi = 0.001$	
4	$\text{NO}_2^- + \cdot\text{OH} \rightarrow \cdot\text{NO}_2 + \text{OH}^- (k = 1.0 \times 10^{10} \text{ M}^{-1} \text{ s}^{-1})$	Mack and Bolton, 1999; Pang et al., 2019a
5	$\text{O}_2^{\cdot-} + \text{NO}_2^- + 2\text{H}^+ \rightarrow \cdot\text{NO}_2 + \text{H}_2\text{O}_2$	Vione et al., 2001; Pang et al., 2019a
6	$\text{NO}_2^- + h\nu \rightarrow \cdot\text{NO} + \text{O}^-; \phi_{\text{OH},300} = 6.7(\pm 0.9)\%$	Fischer and Warneck, 1996; Mack and Bolton, 1999; Pang et al., 2019a
7	$\cdot\text{NO} + \text{O}_2 \leftrightarrow \cdot\text{ONOO}$	Goldstein and Czapski, 1995a; Pang et al., 2019a
8	$\cdot\text{ONOO} + \cdot\text{NO} \rightarrow \text{ONOONO}$	
9	$\text{ONOONO} \rightarrow 2\cdot\text{NO}_2$	
10	$\text{NO}_3^- + h\nu \rightarrow \cdot\text{NO}_2 + \text{OH} \text{ (reactions 1 \& 2)} \rightarrow \text{HOONO} \xrightleftharpoons{h\nu} \cdot\text{NO} + \cdot\text{HO}_2$ ( $pK_a = 6.8$ )	Goldstein et al., 2005; Vione et al., 2005; Sturzbecher-Höhne et al., 2009; Abida et al., 2011; Wang et al., 2021
11	$\cdot\text{HO}_2 \rightleftharpoons \text{H}^+ + \text{O}_2^{\cdot-} \xrightleftharpoons{\text{NO}_2} \text{OONO}_2^- \xrightarrow{\text{H}_2\text{O}} \text{O}_2 + \text{NO}_2^- \xrightleftharpoons{+\text{H}^+} \text{HONO}$ ( $pK_a = 4.8$ ) ( $pK_a = 3.2$ )	Lammel et al., 1990; Goldstein et al., 1998; Wang et al., 2021
12	$\text{O}_2^{\cdot-} + \text{NO} \rightleftharpoons \text{OONO}^- \begin{cases} \xrightarrow{\text{HOONO}} \text{NO}_2^- + \text{HOONO}_2 \rightleftharpoons \text{OONO}_2^- + \text{H}^+ \\ \xrightarrow{\quad\quad\quad} \text{NO}_3^- \end{cases}$ ( $pK_a = 5.9$ )	Goldstein and Czapski, 1995b; Wang et al., 2021
13	$\text{HNO}_2 + h\nu \rightarrow \cdot\text{NO} + \text{OH}; \phi_{\text{OH},300} = 36.2(\pm 4.7)\%$	Fischer and Warneck, 1996; Kim et al., 2014; Pang et al., 2019a
14	$\text{HOONO} \rightarrow \cdot\text{NO}_2 + \cdot\text{OH} (k = 0.35 \pm 0.03 \text{ s}^{-1})$	Goldstein et al., 2005; Pang et al., 2019a
15	$\text{HNO}_2 + \cdot\text{OH} \rightarrow \cdot\text{NO}_2 + \text{H}_2\text{O} (k = 2.6 \times 10^9 \text{ M}^{-1} \text{ s}^{-1})$	Kim et al., 2014; Pang et al., 2019a
16	$(\text{CH}_3)_2\text{CHOH} + \cdot\text{OH} \rightarrow (\text{CH}_3)_2\text{COH}^\cdot + \text{H}_2\text{O}$	Warneck and Wurzinger, 1988; Pang et al., 2019a
17	$(\text{CH}_3)_2\text{COH}^\cdot + \text{O}_2 \rightarrow (\text{CH}_3)_2\text{CO} + \cdot\text{HO}_2$	
18	$\cdot\text{OH} + \text{HCO}_3^- \rightarrow \text{CO}_3^{\cdot-} + \text{H}_2\text{O} (k = 8.5 \times 10^6 \text{ M}^{-1} \text{ s}^{-1})$	Wojnárovits et al., 2020
19	$\cdot\text{OH} + \text{CO}_3^{2-} \rightarrow \text{CO}_3^{\cdot-} + \text{OH}^- (k = 3.9 \times 10^8 \text{ M}^{-1} \text{ s}^{-1})$	
20	$^3\text{C}^* + \text{HCO}_3^- \rightarrow \text{CO}_3^{\cdot-} + \text{H}^+ + \text{C}^\cdot$ ( $k = 10^6\text{-}10^7 \text{ M}^{-1} \text{ s}^{-1}$ ; $^3\text{C}^*$ : triplet aromatic ketones)	Canonica et al., 2005
21	$^3\text{C}^* + \text{CO}_3^{2-} \rightarrow \text{CO}_3^{\cdot-} + \text{C}^\cdot$ ( $k = 10^6\text{-}10^7 \text{ M}^{-1} \text{ s}^{-1}$ ; $^3\text{C}^*$ : triplet aromatic ketones)	

1096



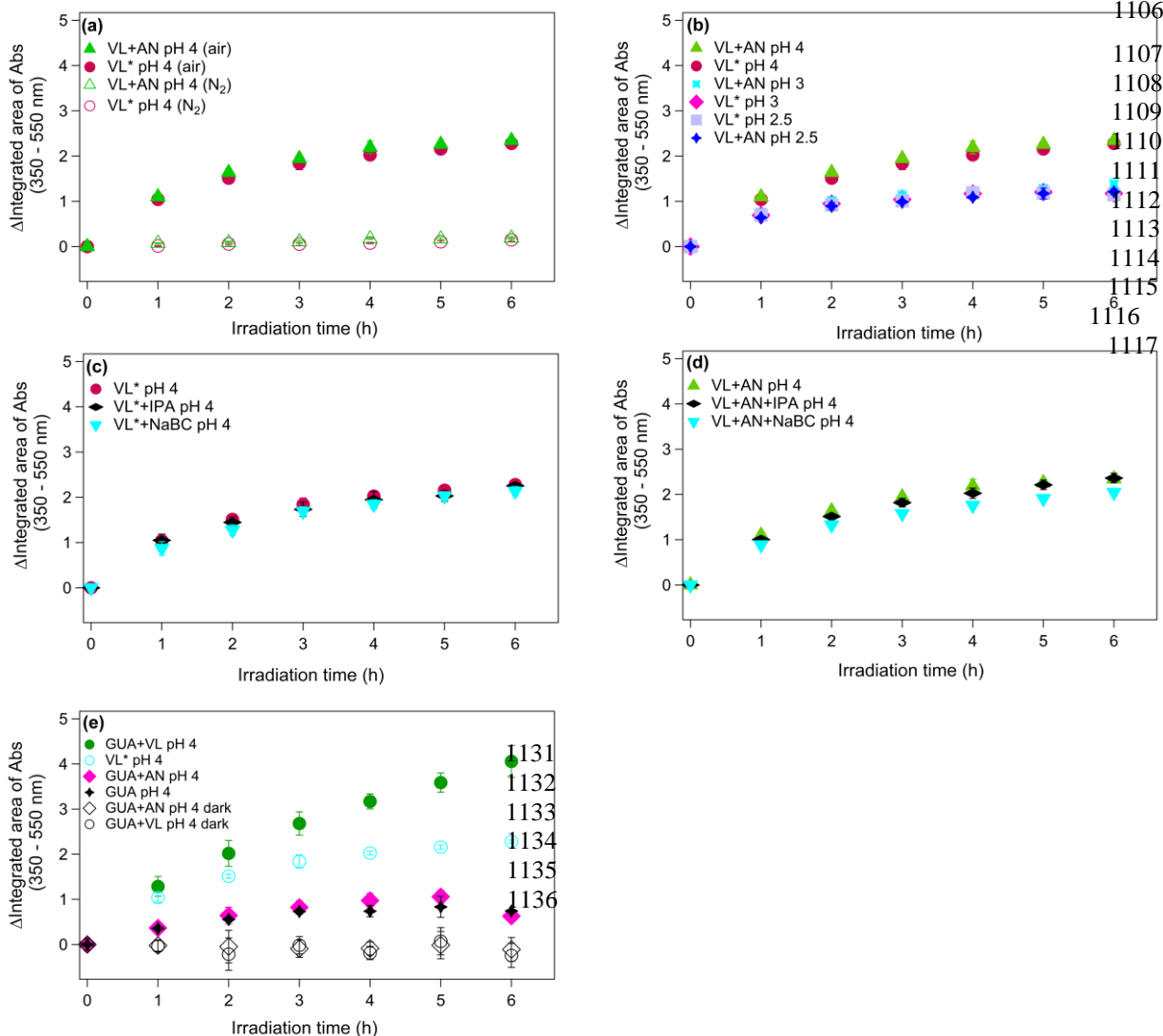
1097

1098 **Figure 1.** Reconstructed mass spectra of assigned peaks from (a) VL\* pH 4 (N<sub>2</sub>-saturated; A6), (b) VL+AN pH 4 (N<sub>2</sub>-  
 1099 saturated; A8), (c) VL\* pH 4 (air-saturated; A5), (d) VL+AN pH 4 (air-saturated; A7), (e) VL\* pH 3 (air-saturated; A3), (f)



1100 VL+AN pH 3 (air-saturated; A4), (g) VL\* pH 2.5 (air-saturated; A1), and (h) VL+AN pH 2.5 (air-saturated; A2) after 6 h  
1101 of simulated sunlight irradiation. The normalized abundance of products was calculated from the ratio of the peak area of the  
1102 product to that of VL (Eq. 2). The 50 most abundant products contributed more than half of the total normalized abundance  
1103 of products, and they were identified as monomers (blue), dimers (green), trimers (red), and tetramers (orange). Grey peaks  
1104 denote peaks with low abundance or unassigned formula. Examples of high-intensity peaks were labeled with the  
1105 corresponding neutral formulas. Note the different scales on the y-axes.





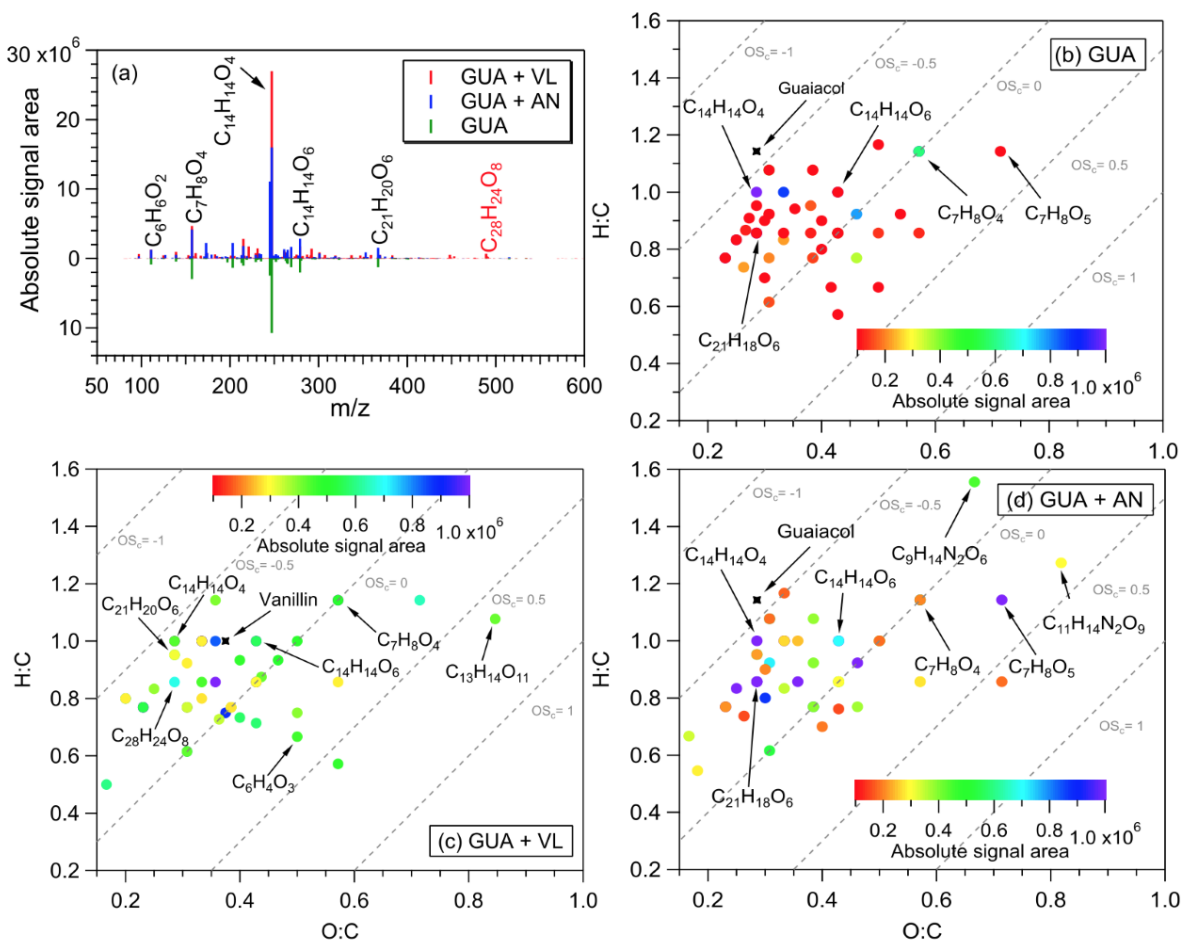
1118  
 1119  
 1120  
 1121  
 1122  
 1123  
 1124  
 1125  
 1126  
 1127  
 1128  
 1129  
 1130

1137  
 1138  
 1139  
 1140  
 1141  
 1142  
 1143

1144 **Figure 2.** (a-d) Increase in light absorption under different experimental conditions for direct photosensitized oxidation of  
 1145 VL (VL\*) and nitrate-mediated VL photo-oxidation (VL+AN): (a) Effect of secondary oxidants from VL triplets on VL\*  
 1146 and VL+AN at pH 4 under N<sub>2</sub>- (A6, A8) and air-saturated (A5, A7) conditions. (b) Effect of pH on VL\* and VL+AN at pH  
 1147 2.5 (A1, A2), 3 (A3, A4), and 4 (A5, A7) under air-saturated conditions. (c) Effect of VOCs and inorganic anions: IPA (A9)  
 1148 and NaBC (A10) on VL\* at pH 4 under air-saturated conditions. (d) Effect of VOCs and inorganic anions: IPA (A11) and  
 1149 NaBC (A12) on VL+AN at pH 4 under air-saturated conditions. (e) Increase in light absorption during direct GUA  
 1150 photodegradation (A17) and photo-oxidation of GUA in the presence of VL (GUA+VL; A18) or nitrate (GUA+AN; A19) at  
 1151 pH 4 under air-saturated conditions after 6 h of simulated sunlight irradiation. Error bars represent 1 standard deviation.



1152

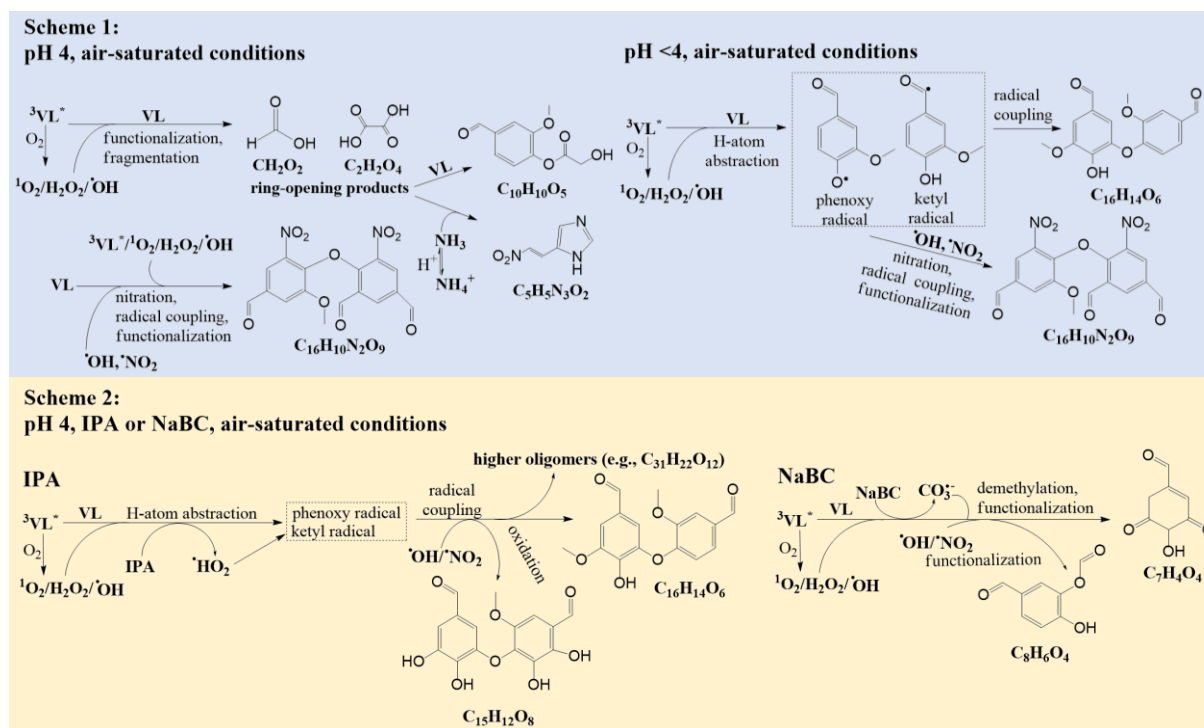


1153

1154 **Figure 3.** (a) Reconstructed mass spectra of assigned peaks from the direct GUA photodegradation (A17) and photo-  
1155 oxidation of GUA in the presence of VL (GUA+VL; A18) or nitrate (GUA+AN; A19) at pH 4 under air-saturated conditions  
1156 after 6 h of simulated sunlight irradiation. The y-axis is the absolute signal area of the products. Examples of high-intensity  
1157 peaks were labeled with the corresponding neutral formulas. (b-d) van Krevelen diagrams of the 50 most abundant products  
1158 from the (b) direct photodegradation of GUA (A17), (c) GUA+VL (A18), and (d) GUA+AN (A19) at pH 4 under air-  
1159 saturated conditions after 6 h of simulated sunlight irradiation. The color bar denotes the absolute signal area. The grey  
1160 dashed lines indicate the carbon oxidation state values (e.g., OS<sub>c</sub> = -1, 0, and 1).



1161



1162

1163

1164 **Figure 4.** Potential photo-oxidation pathways of VL via direct photosensitized reactions and in the presence of nitrate to  
1165 illustrate the effects of secondary oxidants from VL triplets, pH, and the presence of VOCs (IPA) and inorganic anions  
1166 (NaBC). Product structures were proposed based on the molecular formulas, DBE values, and MS/MS fragmentation  
1167 patterns. The molecular formulas presented were the most abundant products or products with a significant increase in  
1168 normalized abundance.